Neuropeptide Y-expressing dorsal horn inhibitory interneurons gate spinal pain and itch signalling

Kieran A. Boyle[1,3], Erika Polgár[1,3], Maria Gutierrez-Mecinas[1,3], Allen C. Dickie[1,3], Andrew H. Cooper[1], Andrew M. Bell[1], M. Evelline Jumolea[1], Adrian Casas-Benito[1], Masahiko Watanabe[2], David I. Hughes[1], Greg A. Weir[1], John S. Riddell[1] and Andrew J. Todd[1]*

[1]School of Physiology and Neuroscience, College of Medical, Veterinary and Life Sciences, University of Glasgow, Glasgow G12 8QQ, UK

[2]Department of Anatomy, Hokkaido University School of Medicine, Sapporo 060-8638, Japan

[3]Equal contribution

*Corresponding Author: Andrew.Todd@glasgow.ac.uk

Click here to enter text.

ABSTRACT

Somatosensory information is processed by a complex network of interneurons in the spinal dorsal horn. It has been reported that inhibitory interneurons that express neuropeptide Y (NPY), either permanently or during development, suppress mechanical itch, with no effect on pain. Here we investigate the role of interneurons that continue to express NPY (NPY-INs) in adulthood. We find that chemogenetic activation of NPY-INs reduces behaviours associated with acute pain and pruritogen-evoked itch, whereas silencing them causes exaggerated itch responses that depend on cells expressing the gastrin-releasing peptide receptor. As predicted by our previous studies, silencing of another population of inhibitory interneurons (those expressing dynorphin) also increases itch, but to a lesser extent. Importantly, NPY-IN activation also reduces behavioural signs of inflammatory and neuropathic pain. These results demonstrate that NPY-INs gate pain and itch transmission at the spinal level, and therefore represent a potential treatment target for pathological pain and itch.

Click here to enter text.

INTRODUCTION

The spinal dorsal horn represents the entry point into the CNS for somatosensory information from the trunk and limbs. This information is relayed via projection cells to supraspinal sites, where it leads to perceptions, including pain and itch[1-3]. However, projection cells represent only ~1% of dorsal horn neurons, with the vast majority comprising excitatory and inhibitory interneurons that are arranged into local microcircuits that process somatosensory information. Altered function of these circuits contributes to chronic pain and pruritus (itch)[4,5]. Dysregulation of inhibitory circuits has attracted particular interest, as broad disruption of spinal inhibitory signalling produces behaviours reminiscent of symptoms in patients suffering from chronic pain or pruritus[6-9].

We have described a molecular classification scheme that assigns the inhibitory interneurons in mouse superficial dorsal horn (SDH; laminae I-II) to five largely non-overlapping populations, based on expression of calretinin (CR), parvalbumin (PV), neuronal nitric oxide synthase (nNOS), dynorphin and galanin (Dyn/Gal) or neuropeptide Y (NPY)[10]. This scheme has since been validated and extended by large-scale transcriptomic studies[11,12]. These molecularly-defined interneuron populations appear to be functionally distinct as they display differential activation profiles in response to noxious and innocuous stimuli[11-13]. A major advantage of this approach is that it allows investigation of the function of different populations through targeted manipulation with techniques such as chemogenetics, optogenetetics and toxin-mediated silencing or ablation. Studies of this type have implicated the PV interneurons in preventing tactile allodynia[14,15], the nNOS interneurons in gating both mechanical and thermal inputs[16], and the Dyn/Gal population in suppressing mechanical pain and pruritogen-evoked itch[16,17]. Ablation or silencing of dorsal horn NPY-lineage neurons (i.e. cells that express NPY transiently during development or persistently into adulthood) has been reported to cause spontaneous itching behaviours and enhancement of touch-evoked (mechanical) itch, without affecting pruritogen-evoked itch or pain behaviours[18]. This has led to the view that the main function of the NPY cells is suppression of mechanical itch[19-24]. This limited role for NPY interneurons is surprising for several reasons: (1) they account for one-third of all inhibitory interneurons in SDH[10], (2) they innervate a population of nociceptive projection cells that belong to the anterolateral system (ALS)[13,25-27], (3) while

Click here to enter text.

mechanical itch is restricted to hairy skin, NPY-expressing neurons are present throughout the dorsal horn, including areas innervated from glabrous skin[10,28] and (4) NPY itself has a role in modulating chronic pain[29]. As noted above, the approach used by Bourane et al[18] targeted a broad population of inhibitory interneurons that express NPY during development, as well as those that express NPY in adulthood. Tashima et al[30] recently attempted to target NPY-INs by injecting adeno-associated viruses (AAVs) with a *Npy* promoter into the rat spinal cord. However, expression was largely restricted to lamina IIo (even though many NPY cells are found in other laminae) and fewer than half of the targeted cells contained either NPY or its mRNA. Therefore, the role of those dorsal horn interneurons that continue to express NPY (NPY-INs) remains unclear.

Here we use intraspinal injections of AAVs carrying Cre-dependent expression cassettes into young adult NPY::Cre mice to target dorsal horn NPY-INs. We demonstrate that this technique can be used to manipulate inhibitory interneurons that express NPY in adulthood, while avoiding those cells that transiently express NPY during development. We show that chemogenetic activation of dorsal horn NPY-INs suppresses acute mechanical and thermal nocifensive behaviours, as well as those resulting from pruritogen-evoked itch, and reduces activity in spinal networks that process nociceptive and pruritoceptive information. Furthermore, NPY-IN activation abolishes mechanical and thermal hypersensitivity in models of inflammatory and neuropathic pain. Finally, we show that silencing of NPY-INs results in spontaneous itch and an exaggerated response to pruritogens, and that this depends on a circuit involving GABAergic input from NPY-INs to excitatory interneurons that express the gastrin-releasing peptide receptor (GRPR). Together these results demonstrate that dorsal horn NPY-INs have a far broader role than previously suggested, since they gate transmission of nociceptive and pruriceptive information. They therefore represent a potential target for the development of new treatments for pain and itch.

RESULTS

Click here to enter text.

Cre-dependent AAV injections in young adult NPY::Cre mice target dorsal horn inhibitory NPY interneurons and avoid transient NPY-expressing cells.

We initially assessed the suitability of using intra-spinal injection of AAVs encoding Cre-dependent constructs in RH26 NPY::Cre mice (the line used by Bourane et al[18]) to target NPY-INs in the dorsal horn. We first performed RNAscope fluorescent *in situ* hybridisation (FISH) to compare *Cre* and *Npy* mRNA expression in lumbar spinal cord sections from young adult NPY::Cre mice. Across laminae I-III 91.6% ± 0.3% of cells classed as *Cre*-positive cells were also *Npy*-positive, and these accounted for 62.1% ± 0.6% of *Npy*-positive cells, demonstrating that Cre expression in the NPY::Cre line faithfully captures the majority of NPY-INs in the adult dorsal horn (Figures 1A and 1B). Accordingly, injection of either AAV.flex.tdTomato (tdTom) or AAV.flex.eGFP (both serotype 1 with CAG promoter, see Key Resources Table) into the lumbar dorsal horn of adult NPY::Cre mice (Figure 1C) resulted in fluorescent protein (FP) expression matching that previously reported for NPY neurons[10,26], with cell bodies concentrated in laminae I-III (Figure 1D). The great majority of FP-expressing neurons in laminae I-III were immunoreactive (IR) for NPY (78.5% ± 3.6%), and these accounted for 74.6% ± 1.9% of the NPY-IR neurons in this area (Figures 1D and 1E).

We then crossed NPY::Cre mice with the Cre-dependent reporter line Ai9 (to label all NPY lineage neurons with tdTomato) and injected AAV.flex.eGFP into the lumbar dorsal horn of these mice, to target cells that continued to express NPY (Figures 1F and Figure 1 – figure supplement 1A). In these animals, tdTom-positive cells were seen throughout the dorsal horn, and were much more numerous than eGFP-expressing cells in the region of the injection site (Figure 1G). All tdTom-labelled cells were immunoreactive for the transcription factor Pax2 (Figure 1 – figure supplement 1B), which is expressed by all dorsal horn inhibitory neurons in rodents[7,31], and these accounted for 40.8% ± 10.0% of Pax2 cells in laminae I-III. Virtually all eGFP-expressing neurons within this region were tdTom-positive (97.8% ± 0.2%), but these only accounted for 51.1% ± 3.5% of the tdTom-positive population (Figures 1H and 1I). In agreement with the data presented above, the great majority tdTom+;eGFP+ neurons were found to be NPY-IR (85.2% ± 0.2%), and these accounted for 67.0% ± 6.3% of the NPY-IR cells in laminae I-III. In contrast, only 32.1% ± 2.1% of the tdTom+;eGFP-negative cells displayed NPY immunoreactivity,

Click here to enter text.

126 corresponding to just 24.1% ± 2.7% of all NPY-IR interneurons (Figures 1H and 1I).
127 Overall, 58.3% ± 0.9% of tdTom+ neurons were NPY-immunoreactive.
128 These results suggest that transient Cre expression occurs in a broad population
129 of dorsal horn inhibitory interneurons in NPY::Cre mice, presumably driven by NPY
130 expression during development. However, Cre expression in adult mice occurs in a
131 much more restricted population of inhibitory interneurons that express NPY
132 persistently. To characterise these cells in relation to the neurochemical populations
133 of inhibitory interneurons that we had identified in the SDH[10], we focussed our
134 analysis on laminae I-II and compared the expression of the different neurochemical
135 markers between the tdTom+;eGFP+ and tdTom+;eGFP-negative cells. Within this
136 region, 85.8% ± 2.5% of tdTom+;eGFP+ cells were NPY-IR, while approximately
137 10%, 3% and 1% expressed galanin, nNOS or PV, respectively (Figure 1 – figure
138 supplement 1C). This is in good agreement with the degree of overlap between
139 these markers and NPY that we have previously described[10]. Surprisingly, 23.7% ±
140 7.0% of tdTom+;eGFP+ cells expressed CR (Figure 1 – figure supplement 1C),
141 which has previously been reported to show minimal overlap with NPY-IR[32].
142 Nonetheless tdTom+;eGFP+ cells are largely restricted to the NPY+ population of
143 inhibitory interneurons. In contrast, tdTom+;eGFP-negative neurons were much
144 more broadly spread across four of the populations, with approximately 28%
145 expressing NPY, 44% expressing CR and 24% each expressing galanin or nNOS,
146 although virtually none (1.4% ± 1.4%) expressed PV (Figure 1 – figure supplement
147 1C).
148 Because we intended to use Cre-dependent expression of the excitatory
149 DREADD hM3Dq[7,16] to activate NPY-INs, we also assessed targeting of this receptor
150 to the appropriate interneurons following injection of AAV.flex.hM3Dq-mCherry into
151 the lumbar dorsal horn of adult NPY::Cre mice (Figure 1 – figure supplement 1D).
152 hM3Dq-mCherry-expressing cells in the SDH displayed a near-identical pattern in
153 terms of co-localisation with inhibitory interneuron markers to that of the eGFP+ cells
154 following AAV.flex.eGFP injection (Figure1 – figure supplement 1E and 1F). For the
155 mCherry+ cells, 90.5% ± 6.2% co-expressed NPY (accounting for 66.1% ± 4.8% of
156 all NPY interneurons) and there was little or no overlap with the galanin, nNOS and
157 PV populations (Figure 1 – figure supplement 1E and 1F). Again, significant overlap
158 was observed between hM3Dq-mCherry- and CR-positive cells, with 28.0% ± 1.5%

159 of mCherry-labelled cells displaying CR-IR. NPY-IR was detected in 93.1% ± 3.7% of
160 mCherry+;CR+ cells in sections co-stained with NPY antibody (Figure 1 – figure
161 supplement 1E), demonstrating that this represents NPY::Cre-driven recombination
162 in interneurons co-expressing NPY and CR, rather than ectopic recombination in
163 CR+;NPY-negative interneurons. The level of NPY-IR in the CR cells was generally
164 very low (Figure 1 – figure supplement 1E), which probably explains why this overlap
165 was not detected previously[32]. As expected, virtually all mCherry-labelled cells were
166 inhibitory (97.4% ± 2.6% Pax2-positive), and these accounted for a quarter of all
167 inhibitory interneurons in the SDH (Figure 1 – figure supplement 1F). Crucially, no
168 mCherry-labelled cells were observed in the ipsi- or contralateral L3, L4 or L5 DRG
169 of four AAV.flex.hM3Dq-mCherry-injected NPY::Cre mice (data not shown), as would
170 be expected from the lack of NPY expression in uninjured mouse DRG neurons[33].
171 Collectively these results demonstrate that injection of AAVs encoding Cre-
172 dependent constructs into the dorsal horn of adult NPY::Cre mice allows specific
173 targeting of most inhibitory interneurons that persistently express NPY, and avoids
174 capturing a broader population of inhibitory interneurons that express NPY
175 transiently during development.
176
177 **Activation of inhibitory NPY interneurons reduces activity in dorsal horn**
178 **circuits recruited by nociceptive and pruritic stimuli.**
179 We initially assessed the efficacy of our chemogenetic strategy to activate NPY-
180 INs in NPY::Cre mice injected with AAV.flex.hM3Dq-mCherry by comparing
181 expression of the activity marker Fos two hours after administration of the hM3Dq
182 ligand clozapine-N-oxide (CNO) or vehicle (Figure 2 – figure supplement 1A). Only
183 8.8% ± 4.7% of mCherry-labelled cells in laminae I-III displayed Fos-IR in vehicle-
184 treated animals, but this rose dramatically to 82.9% ± 2.5% in CNO-treated mice
185 (Figure 2 – figure supplement 1B and 1C). Of these mCherry+;Fos+ cells, 87.5% ±
186 3.1% displayed detectable NPY immunoreactivity, and these accounted for 53.9% ±
187 1.2% of all NPY-IR neurons (Figure 2 – figure supplement 1D and 1E). Surprisingly,
188 we also observed a small but significant increase in the proportion of mCherry-
189 negative cells that expressed Fos following CNO (from 2.7% ± 0.3% in vehicle-
190 treated to 5.8% ± 1.0% in CNO-treated mice), and this increase was entirely
191 restricted to inhibitory interneurons (Figure 2 – figure supplement 1C). A significant

192 proportion of these mCherry-negative;Fos+ cells were also NPY-IR (31.3% ± 4.8%;
193 Figure 2 – figure supplement 1E), and these may represent NPY-INs that express
194 hM3Dq-mCherry at a level sufficient for direct CNO-mediated activation, but that is
195 too low for immunohistochemical detection. Alternatively, they may have been
196 indirectly recruited via disinhibition following CNO-mediated activation of hM3Dq-
197 mCherry-expressing NPY-INs. Overall, CNO treatment resulted in Fos expression in
198 65.9% ± 2.8% of all NPY-INs, and these comprised 65.5% ± 3.8% of Fos-expressing
199 cells (Figure 2 – figure supplement 1E). In summary, intraspinal injection of
200 AAV.flex.hM3Dq-mCherry into adult NPY::Cre mice allows chemogenetic activation
201 of two thirds of dorsal horn NPY-INs, and a small proportion of other dorsal inhibitory
202 interneurons.
203 We then assessed the ability of dorsal horn NPY-INs to suppress the transmission
204 of pain- and itch-related information at the circuit level. NPY::Cre mice that had had
205 intraspinal injections of AAV.flex.hM3Dq-mCherry were injected with vehicle or CNO,
206 and then received a noxious heat (hindpaw immersion in 52ºC water) or pruritic
207 (intradermal injection of chloroquine, CQ, in the calf) stimulus ipsilateral to the viral
208 injection under brief general anaesthesia (Figures 2A and 2B). Mice that received the
209 pruritic stimulus were fitted with an Elizabethan collar to prevent Fos induction due to
210 itch-related biting of the leg. Following a two-hour survival period, spinal cord
211 sections were processed for Fos-IR. In vehicle treated animals, the noxious heat and
212 pruritic stimuli resulted in ipsilateral Fos expression in the somatotopically relevant
213 areas of the dorsal horn. Fos+ cells were particularly clustered in the medial half of
214 the SDH following noxious heat, and the middle third of the SDH after CQ, as
215 previously reported[34,35] (Figures 2C and 2D). Accordingly, analysis of Fos expression
216 was performed within these regions of the SDH. In CNO-treated mice there was a
217 clear increase in the proportion of mCherry-labelled cells expressing Fos (Figures
218 2C-2F), presumably due to direct chemogenetic activation of these cells (as
219 described above). However, for both the noxious heat and pruritic stimuli, we
220 observed a significant decrease in the proportion of mCherry-negative cells that were
221 Fos-positive, when compared to vehicle-treated mice (noxious heat: vehicle = 26.7%
222 ± 4.7% vs. CNO = 6.7% ± 1.2%; CQ injection: vehicle = 12.9% ± 4.2% vs. CNO =
223 2.1% ± 0.3%) (Figures 2C-2F). In both cases the decrease was largely restricted to
224 Pax2-negative (excitatory) neurons, although a significant decrease was also

225 observed in Pax2-positive cells in heat-stimulated mice, with a similar trend in CQ-
226 stimulated mice (Figures 2E and 2F).
227 These results demonstrate that activation of NPY-INs inhibits neurons that are
228 normally recruited by noxious or pruritic stimuli in dorsal horn circuits. To investigate
229 the nature of this inhibition in more detail, we performed optogenetic experiments in
230 spinal cord slices from NPY::Cre mice that had received intraspinal injections of
231 AAV.flex.ChR2-eYFP, resulting in expression of eYFP-tagged channelrhodopsin in
232 NPY-INs (Figure 2G). Short pulses of blue light reliably evoked inward currents and
233 action potential firing in all (10/10) eYFP-ChR2+ cells tested (Figure 2 – figure
234 supplement 2A-C). Recordings were made from 41 ChR2-eYFP-negative cells in the
235 SDH (Figures 2G and Figure 2 – figure supplement 2D), with an optogenetically-
236 evoked postsynaptic current (oPSC) being seen in 29 cells (70.7%). In 7 of the cells
237 with oPSCs, bath application of the AMPAr and NMDAr antagonists, NBQX and D-
238 APV, respectively, did not alter the peak amplitude of the current (baseline = -779.8
239 pA ± 267.7 pA vs. NBQX / D-APV = -756.6 pA ± 285.8 pA, p = 0.578, Wilcoxon
240 matched-pairs signed rank test) (Figure 2 – figure supplement 2E and 2F),
241 demonstrating that these were not mediated by glutamate and were therefore
242 optogenetically-evoked IPSCs (oIPSCs). The GABAergic / glycinergic nature of
243 these oIPSCs was investigated by bath application of gabazine and strychnine,
244 respectively (in the presence of NBQX and D-APV). All oIPSCs tested (6/6) were
245 reduced by gabazine, but not strychnine (Figures 2H and 2I), indicating that inhibition
246 is predominantly mediated by GABA. This is consistent with the finding that NPY
247 neurons in laminae I-III are all GABA-IR, but are not enriched with glycine[36]. Taken
248 together, these findings demonstrate that NPY-INs provide a powerful GABAergic
249 inhibitory input to surrounding dorsal horn neurons and reduce the activation of
250 excitatory neurons that are normally recruited by noxious or pruritic stimuli,
251 suggesting that they supress the transmission of pain- and itch-related information in
252 the dorsal horn.
253
254 **Activation of inhibitory NPY interneurons increases acute nocifensive reflex**
255 **thresholds and reduces pruritogen-evoked itch behaviour.**
256 We then looked for behavioural correlates of the NPY-IN-mediated suppression of
257 dorsal horn pain and itch circuits. To do this, we assessed mechanical and thermal

258 nocifensive reflexes, as well as CQ-induced itch behaviour, in NPY::Cre mice that
259 had received unilateral spinal injections of AAV.flex.hM3Dq-mCherry and were then
260 treated with vehicle or CNO (Figure 3A). In vehicle-treated mice, as expected, there
261 were no significant differences between the hindpaws contralateral and ipsilateral to
262 the AAV injection for the 50% mechanical withdrawal threshold (MWT) or for
263 withdrawal latencies to noxious heat or cold. However, in CNO-treated mice
264 nocifensive thresholds/latencies in the ipsilateral paw were significantly increased
265 across all three modalities, demonstrating a generalised anti-nociceptive effect of
266 NPY-IN activation (Figures 3B-3D). CNO-treated mice also spent significantly less
267 time biting the calf area in the 30 minutes following CQ injection than vehicle-treated
268 controls, demonstrating a reduction in pruritogen-evoked itch upon NPY-IN activation
269 (Figure 3E). It has been proposed that when used at high doses, systemic CNO may
270 have off-target effects as a result of conversion to clozapine[37]. We therefore tested
271 the effect of 5mg/kg CNO (the dose used throughout our study) on naïve wild-type
272 mice, and found no change in mechanical or thermal nocifensive thresholds, or on
273 locomotor performance (Figure 3 – figure supplement 1). This confirms that the
274 effects observed in AAV.flex.hM3Dq-mCherry-injected NPY::Cre mice are due to
275 DREADD activation, and not the result of off-target effects of CNO. These findings
276 show that chemogenetic activation of dorsal horn NPY-INs has a broad anti-
277 nociceptive effect across a range of modalities and suppresses pruritogen-evoked
278 itch.
279
280 **Activation of NPY interneurons blocks mechanical and thermal**
281 **hypersensitivity in models of inflammatory and neuropathic pain.**
282 We next assessed the effects of chemogenetically activating NPY-INs in the
283 context of inflammatory and neuropathic pain (Figures 4A, 4D and 4G). Intraplantar
284 CFA resulted in punctate mechanical and heat hypersensitivity of the ipsilateral paw
285 of AAV.flex.hM3Dq-mCherry-injected NPY::Cre mice that received i.p. injection of
286 vehicle prior to behavioural testing. However, the mechanical and heat
287 hypersensitivity were completely blocked in mice treated with CNO, and the heat
288 latencies were significantly increased above the pre-CFA baseline values (Figure 4B
289 and 4C). Vehicle-treated AAV.flex.hM3Dq-mCherry-injected NPY::Cre mice that had
290 undergone spared nerve injury (SNI) also displayed mechanical and heat

291 hypersensitivity of the ipsilateral paw, compared to pre-surgery thresholds. Both the
292 mechanical and heat hypersensitivity were blocked in CNO-treated mice (Figures 4E
293 and 4F). Because *de novo* expression of NPY is known to occur in injured A-fibre
294 afferents following nerve injury[33,38-40], this could result in expression of hM3Dq in
295 these afferents, thus confounding interpretation of our results. We therefore
296 quantified the number of mCherry-labelled cells in the somatotopically-relevant L4
297 and L5 DRG four weeks following SNI surgery in 4 mice (Figure 4 – figure
298 supplement 1). As expected, no labelled cells were observed contralateral to the
299 AAV injection and SNI surgery in either DRG in any of the mice. A few mCherry-
300 labelled cells were observed in both L4 and L5 DRG on the ipsilateral side (cells per
301 DRG: L4 = 12.5 ± 2.3, L5 = 17.5 ± 3.6; Figure 4 – figure supplement 1). Because the
302 numbers of A-fibre sensory neurons within the mid-lumbar DRG are estimated to be
303 in the thousands in mice[41,42], it is highly unlikely that CNO-mediated activation of the
304 very few hM3Dq-expressing cells observed in the L4 and L5 DRG following SNI
305 would contribute to the blockade of neuropathic pain that we observed. We therefore
306 conclude that this effect is due to activation of spinal inhibitory NPY-INs. We also
307 assessed mCherry expression in the L4 and L5 DRG of 5 CFA-treated
308 AAV.flex.hM3Dq-mCherry-injected NPY::Cre mice, 3 days following CFA injection. In
309 contrast to nerve injury, neuropeptide upregulation is not observed in rodent DRG
310 under inflammatory conditions[33,40]. As expected, we observed no mCherry-labelled
311 cells in the contra- or ipsilateral L4 or L5 DRG of these mice (data not shown).
312 Spinal NPY signalling has been implicated in the suppression of neuropathic pain
313 through inhibition of NPY Y1 receptor (Y1R)-expressing excitatory interneurons in
314 the dorsal horn[29,43,44]. Therefore the suppression of neuropathic hypersensitivity that
315 we observed during chemogenetic activation of NPY-INs could be due to GABAergic
316 transmission, NPY signalling, or a combination of both. To assess the potential role
317 of Y1R signalling, we systemically co-administered CNO and the Y1R-selective
318 antagonist BMS 193885[21] prior to behavioural testing in AAV.flex.hM3Dq-mCherry-
319 injected NPY::Cre mice that had undergone SNI surgery. Administration of the Y1R
320 antagonist had no effect on the CNO-mediated suppression of tactile and heat
321 hypersensitivity in these mice (Figures 4E and 4F), suggesting that action of NPY on
322 Y1 receptors is not required for this effect.

323 In addition to evoked hypersensitivity, peripheral nerve injury induces ongoing
324 neuropathic pain in rodents, as well as engaging affective-emotional responses to
325 pain[45]. To determine the contribution of NPY-INs to ongoing pain we tested whether
326 CNO induced conditioned place preference (CPP) in a separate cohort of
327 AAV.flex.hM3Dq-mCherry-injected NPY::Cre mice following SNI surgery (Figure 4G).
328 A wildtype control group that had undergone SNI was also included to test for any
329 possible preference of (or aversion to) the effects of CNO that could have resulted
330 from off-target effects independent of DREADD activation. CNO did not induce
331 preference or aversion in either of these experimental groups (Figures 4H and 4I,
332 Figure 4 – figure supplement 2A and 2B). However, using the same experimental
333 setup we observed preference for a chamber paired with gabapentin in mice that had
334 undergone SNI (Figure 4 – figure supplement 2C and 2D), showing that the CPP
335 method was sufficiently sensitive to detect ongoing neuropathic pain. Together,
336 these findings suggest that activating NPY-INs does not alleviate ongoing pain in the
337 SNI model. We also assessed SNI-induced cold hypersensitivity in the cohort of
338 AAV.flex.hM3Dq-mCherry-injected NPY::Cre mice that were used for CPP testing
339 (Figure 4G). We observed a marked increase in the duration of the response to an
340 acetone droplet applied to the ipsilateral hindpaw relative to the pre-SNI baseline
341 when the mice had been dosed with a vehicle control. Administration of CNO
342 completely blocked this hypersensitivity, demonstrating a reversal of SNI-induced
343 cold allodynia when NPY-INs are activated. This result also demonstrates that the
344 lack of CPP in the chemogenetic experiments was not due to a failure to activate
345 NPY-INs.
346 In summary, chemogenetic activation of NPY-INs supresses both mechanical and
347 thermal hypersensitivity in models of inflammatory and neuropathic pain, and the
348 suppression of neuropathic hypersensitivity appears to be mediated predominantly
349 by GABAergic transmission from NPY-INs. However, NPY-IN activation does not
350 appear to affect ongoing pain in the neuropathic model.
351
352 **Toxin-mediated silencing of NPY interneurons causes spontaneous itch and**
353 **enhances pruritogen-evoked itch but does not alter nocifensive reflexes.**
354 We then tested whether tetanus toxin light chain (TeLC)-mediated silencing of
355 NPY-INs following spinal injection of AAV.flex.TeLC.eGFP into NPY::Cre mice

356 altered pain- or itch-related behaviours (Figure 5A and Figure 5 – figure supplement
357 1A). Immunohistochemical assessment of the overlap of NPY and GFP expression
358 in these mice demonstrated a very similar specificity and efficacy of expression in
359 NPY-INs to that described above for other viral constructs. In animals injected with
360 AAV.flex.TeLC.eGFP 82.6% ± 5.0% of GFP-positive cells co-expressed NPY and
361 61.7% ± 3.5% of NPY-positive cells co-expressed GFP (Figure 5 – figure
362 supplement 1F and 1G).
363 Compared to AAV.flex.eGFP-injected controls, AAV.flex.TeLC.eGFP-injected
364 NPY::Cre mice displayed significant enhancement of CQ-induced itch when tested 4
365 to 6 days after AAV injection ($P<0.0001$, 2-way ANOVA with Tukey's post-test,
366 Figure 5B). Approximately two thirds of AAV.flex.TeLC.eGFP-injected mice also
367 developed skin lesions on the ipsilateral hindlimb, within the corresponding
368 dermatomes, by day 7 (Figures 5D and 5E). This phenotype was never observed in
369 the AAV.flex.eGFP-injected controls, and strongly suggests development of
370 spontaneous itch following silencing of NPY-INs. Consistent with this interpretation,
371 we observed a significant increase in the time spent biting the calf prior to CQ
372 injection in AAV.flex.TeLC.eGFP-injected NPY::Cre mice compared to
373 AAV.flex.eGFP-injected mice of the same genotype ($P=0.0014$, 2-way ANOVA with
374 Tukey's post-test, Figure 5C). In contrast to these marked effects on itch-related
375 behaviours, silencing of NPY-INs did not significantly alter punctate tactile or thermal
376 nocifensive thresholds at 4-6 days after AAV injection (Figure 5 – figure supplement
377 1A-1D). Motor co-ordination, as assessed by rotarod, was also unaffected by NPY-
378 IN silencing; however, a small but significant improvement was detected in
379 AAV.flex.eGFP-injected mice relative to their baseline pre-surgery performance,
380 most likely reflecting a mild training effect (Figure 5 – figure supplement 1E). Taken
381 together these findings indicate that tonic activity of NPY-INs suppresses itch, but
382 has no obvious impact on nociceptive thresholds.
383
384 **Increased itch caused by silencing NPY interneurons operates through a**
385 **circuit involving GRPR-expressing excitatory interneurons.**
386 Several studies have shown that GRPR-expressing excitatory dorsal horn
387 interneurons (GRPR-INs) are crucial for pruritogen-evoked itch[46-48], while it has been
388 proposed that they are not required for mechanical itch[18,21] (but see Chen et al[232323]).

389 To assess whether signalling through GRPR-INs was required for the itch-related
390 behaviours that we observed when NPY-INs were silenced, we crossed NPY::Cre
391 and GRPR^{CreERT2} mice and concomitantly silenced NPY-INs and GRPR-INs through
392 spinal injection of AAV.flex.TeLC.eGFP (Figure 5A). AAV.flex.eGFP-injected mice of
393 the same genotype were again used as a control group. NPY::Cre;GRPR^{CreERT2} mice
394 that received injections of AAV.flex.TeLC.eGFP showed no significant difference in
395 CQ-induced itch, compared to AAV.flex.eGFP-injected controls (P=0.34, 2-way
396 ANOVA with Tukey's post-test, Figure 5B). However, when comparing NPY::Cre and
397 NPY::Cre;GRPR^{CreERT2} mice that had received injections of AAV.flex.TeLC.eGFP,
398 the NPY::Cre;GRPR^{CreERT2} mice showed significantly less CQ-induced itch behaviour
399 than NPY::Cre mice (P<0.0001, 2-way ANOVA with Tukey's post-test, Figure 5B).
400 Furthermore, AAV.flex.TeLC.eGFP-injected NPY::Cre;GRPR^{CreERT2} mice did not
401 display a significant increase in spontaneous biting prior to CQ administration
402 (compared to AAV.flex.eGFP-injected controls; P=0.82, 2-way ANOVA with Tukey's
403 post-test, Figure 5C) and never developed skin lesions (Figures 5D and 5E). These
404 data demonstrate that both the spontaneous itch and the increased pruritogen-
405 evoked itch observed following silencing of NPY-INs are at least partly transmitted
406 via GRPR-INs.
407 This led us to ask whether NPY-INs provide direct inhibitory synaptic input to
408 GRPR-INs. To investigate this we performed *ex vivo* patch clamp experiments in
409 spinal cord slices from NPY::Cre;GRPR^{FlpO} mice that had received intraspinal
410 injections of AAV.flex.ChR2-eYFP together with AAV.FRT.mCherry, resulting in
411 expression of eYFP-tagged channelrhodopsin in NPY-INs and mCherry in GRPR-
412 INs (Figure 5F). Recordings were made from 11 mCherry+ cells and all of these
413 exhibited an oIPSC (with no failures) when the slice was illuminated with brief pulses
414 of blue light, with a mean peak oIPSC amplitude of 250.1 pA ± 58.9 pA (Figure 5G).
415 In 3 / 3 of these cells oIPSCs were abolished by the application of TTX and rescued
416 by the addition of 4-AP (Figure 5H), confirming that they were monosynaptic, and
417 therefore that NPY-INs directly inhibit GRPR-INs. The GABAergic / glycinergic
418 nature of the oIPSCs was assessed in three of the cells (Figure 5 – figure
419 supplement 2A-2C). In 2 / 3 cells the oIPSC was gabazine sensitive / strychnine
420 insensitive, indicating GABA-mediated inhibition, while in the other cell the oIPSC
421 was sensitive to both gabazine and strychnine, indicating mixed GABA and glycine

422 inhibition (Figure 5 – figure supplement 2B and 2C). Although Acton et al[21] provided
423 evidence that GRPR-INs lack the Y1R, Chen et al[23] reported that 35% of GRPR cells
424 had *Y1R* mRNA. We therefore tested the effect of bath-applying the Y1R agonist
425 [Leu^{31},Pro^{34}]-neuropeptide Y, while recording from GRPR-INs (Figure 5 – figure
426 supplement 2D). We found that all 10 cells tested failed to show an outward current
427 in response to [Leu^{31},Pro^{34}]-neuropeptide Y (Figure 5 – figure supplement 2E and
428 2F), suggesting that NPY acting on the Y1R is unlikely to have made a significant
429 contribution to the suppression of GRPR cells by NPY-INs. We also investigated
430 inhibitory NPY-IN input to GRPR-INs anatomically. To do this, we quantified the
431 proportion of inhibitory synaptic contacts onto GRPR-INs (labelled through spinal
432 injection of Cre-dependent AAV-Brainbow2 into GRPR^{CreERT2} mice; Figure 5I) at
433 which NPY was present in the presynaptic bouton. Inhibitory synapses were
434 identified by the presence of VGAT-positive presynaptic boutons apposed to puncta
435 of the postsynaptic protein gephyrin. Many of the gephyrin puncta on the GRPR-INs
436 were contacted by NPY-IR boutons, and these accounted for 45.0% ± 1.9% of all
437 inhibitory synapses on the GRPR-INs (Figures 5J and 5K). This was significantly
438 higher than the proportion of inhibitory (VGAT+) boutons in the vicinity of the
439 analysed cells that contained NPY (36.2% ± 2.6%; Figure 5K). Together these data
440 provide strong evidence that NPY-INs selectively target GRPR-INs and generate a
441 powerful GABAergic inhibition of these cells.
442
443 **Toxin-mediated silencing of dynorphin interneurons enhances pruritogen-**
444 **evoked itch.**
445 Dorsal horn inhibitory interneurons that co-express dynorphin and galanin have
446 been implicated in suppression of itch as their activation reduces pruritogen-evoked
447 itch[16,22], while constitutive loss of B5-I neurons, which include this population, results
448 in enhanced pruritogen-evoked itch and skin lesions due to spontaneous
449 scratching[49,50]. In addition, Brewer et al[51] reported that chemogenetic inhibition of
450 dynorphin lineage cells increases pruritogen-evoked itch. Given the well-established
451 role of dynorphin-expressing interneurons (Dyn-INs) in suppressing itch, we
452 compared the effect of silencing these cells on spontaneous and pruritogen-evoked
453 itch with that of silencing the NPY-INs. Although dynorphin is also expressed by a
454 subset of dorsal horn excitatory interneurons, we have shown that these are largely

455 restricted to areas innervated by afferents from glabrous skin[16]. We injected
456 AAV.flex.TeLC.eGFP (or AAV.flex.eGFP as a control) into the dorsal horn of the L3
457 segment of Pdyn^{Cre} mice for these experiments (Figure 6A). This segment was
458 chosen for 2 reasons: (1) it receives input from the region of calf that we used to test
459 the effect of pruritogens, and (2) it receives input exclusively from hairy skin, and
460 therefore the great majority of virally-transfected Dyn-INs are likely to be inhibitory
461 cells (those that co-express dynorphin and galanin)[16].
462 In contrast to the effects of silencing NPY-INs, silencing of Dyn-INs never resulted
463 in skin lesions, and the time spent biting the calf prior to CQ injection appeared to be
464 unaffected (Figure 6B; P=0.7431, 2-way repeated measures ANOVA with Šidák's
465 post-test). This suggests that silencing Dyn-INs does not result in spontaneous itch.
466 Silencing of Dyn-INs did result in enhanced CQ-evoked itch, when compared to
467 AAV.flex.eGFP-injected controls (Figure 6B; P=0.0379, 2-way repeated measures
468 ANOVA with Šidák's post-test). However, this enhancement was markedly less
469 pronounced than that observed following silencing of NPY-INs (compare Figure 6B
470 with Figure 5B). To confirm that the effects of TeLC-mediated silencing resulted from
471 targeting of Cre-expressing cells, we also injected either AAV.flex.TeLC.eGFP or
472 AAV.flex.eGFP into the L3 segments of wild-type mice, and assessed CQ-evoked
473 itch behaviours 4-6 days later (Figure 6 – figure supplement 1A). As expected in
474 these control animals there was no significant difference in the time spent biting the
475 calf between AAV.flex.TeLC.eGFP- or AAV.flex.eGFP-injected mice either before or
476 after injection of CQ (Figure 6 – figure supplement 1B).
477 These findings suggest that while both NPY- and Dyn-INs can suppress itch, the
478 NPY population has a more substantial role in this mechanism. One explanation for
479 this could be that although Dyn-INs form inhibitory synapses onto GRPR cells[22], the
480 density of these synapses is less than that of those arising from the NPY-INs. To test
481 this, we assessed contacts from inhibitory dynorphin cells onto GRPR-INs (Fig 6C-
482 6E), using an antibody against dynorphin B (DynB) and found that these constituted
483 only 20.9% ± 2.2% of the inhibitory synapses on these cells. This did not differ
484 significantly from the proportion of inhibitory boutons that contained DynB in the
485 vicinity of the analysed cells (22.6% ± 1.6%; Figures 6D and 6E). Collectively these
486 results suggest that unlike NPY-INs, Dyn-INs do not preferentially target GRPR-INs.
487 In addition, they contribute a far lower proportion of inhibitory synapses on the

488 GRPR-INs (compared to the NPY-INs), and loss of this input has a much less
489 dramatic effect on itch.
490

491 **DISCUSSION**

492 Inhibitory interneurons in the SDH play an important role in suppressing pain and
493 itch. NPY-expressing cells constitute around a third of the inhibitory neurons in this
494 region and are also present in deeper laminae. Previous studies in which NPY-
495 lineage neurons were ablated demonstrated that these cells are responsible for
496 preventing mechanical itch through a mechanism involving NPY and the Y1
497 receptor[18,21]. Here we show, by selectively activating those cells that continue to
498 express the peptide, that the NPY cells inhibit acute nocifensive reflexes and reduce
499 mechanical and thermal hypersensitivity in both inflammatory and neuropathic pain
500 models. In addition, they strongly suppress itch evoked by chloroquine. Silencing the
501 NPY cells causes spontaneous itch and exaggerated responses to chloroquine, and
502 both of these effects are reduced by simultaneously silencing GRPR-expressing
503 excitatory interneurons, indicating that suppression of itch by the NPY cells operates
504 through downstream GRPR-INs.
505

506 **A broad inhibitory role for NPY cells**

507 Our findings indicate that NPY-INs have a far broader role in suppressing pain-
508 and itch-related behaviours than had been suggested by previous studies that used
509 the same NPY::Cre line[18,20,21]. The differences in experimental findings are likely to
510 result from two methodological issues: (1) the technique used to target cells, and (2)
511 the use of loss-of-function or gain-of-function approaches. In each of these other
512 studies, cells were targeted by an intersectional genetic approach that limited
513 expression to spinal cord and brainstem, but would have included a large additional
514 group of inhibitory neurons that expressed NPY only during development[18]. Here, we
515 used an alternative strategy to restrict expression: intraspinal injection of AAVs
516 coding for Cre-dependent constructs[7,16]. While this approach failed to capture a
517 minority of NPY-expressing neurons, it enabled us to target a large number of these
518 cells. Importantly, expression was restricted to those cells that continue to express
519 NPY. This was confirmed by our finding that up to 85% of the virally transfected cells
520 contained detectable levels of NPY.

Click here to enter text.

521 Other differences in the roles attributed to the NPY cells are likely to depend on
522 whether cells were inactivated (through ablation or synaptic silencing) or
523 chemogenetically activated. In agreement with Bourane et al[18], we found that
524 silencing NPY cells had no effect on acute nociceptive thresholds. However,
525 chemogenetically activating these cells increased thresholds for both thermal and
526 mechanical nocifensive reflexes. Interestingly, Acton et al[21] also observed an anti-
527 nociceptive effect (increased von Frey thresholds and reduced responses to
528 pinprick) when they chemogenetically activated NPY-lineage neurons, but attributed
529 this to ectopic activation of Y1 receptors on primary sensory neurons. However,
530 although Y1 is present in cell bodies of some primary sensory cells, it is not thought
531 to traffic to their central terminals[52,53]. The most likely explanation for discrepancies
532 between the findings of loss-of-function and gain-of-function studies is that although
533 NPY cells have an antinociceptive action, other interneurons provide sufficient
534 inhibition to maintain nocifensive reflexes when NPY cells are silenced. Our findings
535 therefore indicate that NPY-INs have a far broader role in somatosensory processing
536 than was previously recognised.
537
538 **NPY cells suppress spontaneous and pruritogen-evoked itch**
539 Our previous studies[16,49] had implicated dynorphin/galanin cells in suppression of
540 pruritogen-evoked itch. This was based on the findings that *Bhlhb5*$^{-/-}$ mice (which
541 lack these cells) show exaggerated responses to pruritogens[49], and that
542 chemogenetic activation of dynorphin-expressing cells suppressed CQ-evoked itch[16].
543 In support of this, Liu et al[22] subsequently showed that activating galanin-expressing
544 cells also suppresses pruritogen-evoked itch. This anti-pruritic action is likely to
545 involve dynorphin acting on κ-opioid receptors[49] as well as direct inhibition of GRPR
546 cells (which are an integral part of the spinal itch pathway) by GABA and/or glycine
547 released from the dynorphin/galanin cells[22]. Liu et al also showed that ablating
548 galanin-expressing cells enhances pruritogen-evoked itch, and consistent with this
549 we find enhancement of CQ-evoked itch when cells belonging to this population are
550 silenced by injecting AAV.flex.TeLC into Pdyn^{Cre} mice.
551 Here we show that activating NPY cells also strongly suppresses CQ-evoked itch.
552 This is at odds with findings of Acton et al[21], who reported that chemogenetic
553 activation of NPY-lineage neurons failed to alter scratching in response to CQ. There

554 are technical differences between these studies, since Acton et al used a reporter
555 mouse line to express hM3Dq, and injected CQ intradermally behind the ear. The
556 discrepancy between our results may therefore reflect regional differences (hindlimb
557 versus head), higher levels of DREADD expression resulting from viral transfection,
558 and/or differences in the populations targeted (as noted above). Although Bourane et
559 al[18] reported that ablating NPY-lineage neurons had no effect on itch evoked by CQ,
560 we found that synaptic silencing of the NPY cells with TeLC increased CQ-evoked
561 itch, and often resulted in development of skin lesions, presumably secondary to the
562 development of spontaneous itch-related biting that was also observed. In fact, the
563 antipruritic action of the NPY-INs may be more powerful than that of the
564 dynorphin/galanin cells, since TeLC silencing in the $Pdyn^{Cre}$ mouse caused less of
565 an increase in chloroquine-evoked itch behaviour (compared to silencing in the
566 NPY::Cre line) and did not result in the development of spontaneous itch or
567 associated skin lesions.
568
569 **NPY cells operate through a circuit involving GRPR neurons**
570 Both spontaneous and CQ-evoked itch behaviours were suppressed when GRPR
571 and NPY cells were silenced simultaneously, and we show directly, using both
572 anatomical and electrophysiological methods, that the NPY cells provide a strong
573 inhibitory input to GRPR-INs. This indicates that GRPR cells are downstream of the
574 NPY cells (Figure 7A). This inhibitory input to GRPR cells appears to be even more
575 powerful than that originating from the dynorphin/galanin cells, since NPY-
576 immunoreactive boutons accounted for 45% of the inhibitory synapses on the GRPR
577 cells, compared to the 21% from dynorphin-immunoreactive boutons. Consistent with
578 this we found that optogenetic activation of NPY cells elicited oIPSCs in all of the
579 GRPR cells tested. Interestingly, these were of much higher mean amplitude (~250
580 pA), than the ~80 pA oIPSCs reported by Liu et al[22] in GRPR cells when galanin
581 cells were optogenetically activated using a very similar experimental approach. The
582 inhibition of GRPR cells by NPY-INs is likely to be predominantly GABAergic, since
583 oIPSCs were reduced by gabazine in all cells (with one also sensitive to strychnine).
584 Also, consistent with previous evidence showing that the majority of GRPR cells lack
585 Y1 receptors[21,23], we did not detect outward currents in any of the GRPR cells that
586 were tested with a Y1 agonist.

587 Although GRPR-expressing excitatory interneurons have been strongly implicated
588 in itch, we have recently shown that these cells respond to noxious as well as pruritic
589 stimuli, that they correspond morphologically to a class of SDH excitatory
590 interneurons known as vertical cells, and that chemogenetically activating them
591 results in behaviours reflecting both pain and itch[54]. Vertical cells provide input to
592 lamina I projection neurons[55], and are thought to form an integral part of circuits that
593 underlie both normal and pathological pain[17,56,57]. It is already known that axons of
594 NPY cells directly innervate lamina I projection cells, as well as a population of
595 nociceptive projection neurons in laminae III-V of the dorsal horn[27,58]. This direct
596 input to ALS projection neurons will presumably contribute to the antinociceptive
597 action of the NPY cells. The present findings suggest that the powerful inhibitory
598 GABAergic NPY-GRPR circuit that we have identified may provide an additional
599 mechanism that would subserve not only the alleviation of itch, but also the
600 suppression of nocifensive reflexes and the reduction of hypersensitivity in persistent
601 pain states (Figure 7B).
602
603 **NPY cells suppress hypersensitivity in persistent pain states**
604 Importantly, in addition to its effect on acute nocifensive reflexes and itch,
605 activating NPY cells also blocked thermal and mechanical hypersensitivity in both
606 inflammatory and neuropathic pain states. In the SNI model, we found that
607 administration of a Y1 antagonist had no effect on the reversal of mechanical and
608 heat hypersensitivity when NPY cells were activated. NPY acting on Y1 receptors
609 expressed by spinal neurons is known to reduce signs of neuropathic pain[29,43,59];
610 however, it appears that chemogenetic activation of NPY cells generated GABAergic
611 inhibition that was sufficiently powerful to reverse the hypersensitivity independently
612 of Y1 signalling. Interestingly, our CPP findings suggest that activating NPY neurons
613 did not suppress on-going pain in the SNI model, implying that on-going and evoked
614 components of neuropathic pain operate through different circuits at the spinal cord
615 level.
616 Previous studies have tested the effects of chemogenetically activating other
617 inhibitory interneuron populations on persistent pain states. Glycinergic cells account
618 for the majority of inhibitory interneurons in deep dorsal horn and are largely
619 separate from the NPY-INs[36,60]. Foster et al[7] showed that activating these cells

620 reduced responses to acute thermal and mechanical noxious stimuli and suppressed
621 mechanical hypersensitivity in the chronic constriction injury model. Activation of PV-
622 expressing inhibitory interneurons reduced inflammatory and neuropathic
623 mechanical allodynia, but had no effect on heat hypersensitivity[15]. A recent study by
624 Albisetti et al[61] found that activating a population of dorsal horn inhibitory
625 interneurons defined by expression of *Kcnip2* suppressed cold allodynia in a
626 neuropathic model. However, our findings apparently provide the first evidence that
627 activating dorsal horn inhibitory interneurons can suppress heat hypersensitivity, in
628 addition to cold and mechanical allodynia, in persistent pain states. A population of
629 NPY-expressing inhibitory interneurons with a similar laminar location has recently
630 been identified in human spinal cord[62]. These cells therefore provide an attractive
631 target for the treatment of neuropathic pain, particularly for the significant cohort of
632 patients who experience thermal hyperalgesia[63].
633

634 **MATERIALS AND METHODS**

635

636 **Key resources table**

Reagent or resource	Source	Identifier
Mouse lines		
STOCK Tg(Npy-cre)RH26Gsat/Mmucd (*NPY::Cre*)	GENSAT / MMRRC	Cat#: 34810-UCD RRID: MMRRC_34810-UCD
B6.Cg-Gt(ROSA)26Sor$^{tm9(CAG\text{-}tdTomato)Hze}$/J (Ai9)	Prof. Hongkui Zheng; available from The Jackson Laboratory, ME, USA	Cat#: 007909 RRID: IMSR_JAX:007909
GRPR-iCreERT2 (*Grpr^{CreERT2}*)	Dr. Yan-Gang Sun	Liu et al.(2019), PNAS 116, 27011-27017
GRPR-FlpO (*Grpr^{FlpO}*)	Dr. Yan-Gang Sun	Mu et al. (2017), Science 357, 695-699
B6;129S-Pdyn$^{tm1.1(cre)Mjkr}$/LowlJ (*Pdyn^{Cre}*)	The Jackson Laboratory, ME, USA	Cat#: 027958 RRID: IMSR_JAX:027958
AAV constructs		
AAV1 pCAG-FLEX-EGFP-WPRE (AAV.flex.eGFP; 1.72 x 10^9 GC)	Penn Vector Core, PA, USA; available from Addgene, MA, USA (deposited by Hongkui Zeng)	Cat#: 51502 RRID: Addgene_51502 Oh et al. (2014), Nature 508, 207-214
AAV1 pCAG-FLEX-tdTomato-WPRE (AAV.flex.tdTomato; 1.76 x 10^9 GC)	Penn Vector Core, PA, USA; available from Addgene, MA, USA (deposited by Hongkui Zeng)	Cat#: 51503 RRID: Addgene_51503 Oh et al. (2014), Nature 508, 207-214
pAAV1-EF1a-double floxed-hChR2(H134R)-EYFP-WPRE-HGHpa	Penn Vector Core, PA, USA; available from Addgene, MA,	Cat#: 20298 RRID: Addgene_20298

(AAV.ChR2-eYFP; 5.09 x 10^8 GC)	USA (deposited by Karl Deisseroth)	
rAAV2/hSyn-DIO-hm3D-mcherry (AAV.flex.hM3Dq-mCherry; 3.8 x 10^8 GC)	University of North Carolina Vector Core, NC, USA; available from Addgene, MA, USA (deposited by Bryan Roth)	Cat#: 44361 RRID: Addgene_44361 Krashes et al. (2011), J Clin Invest. 121, 1424-1428
ssAAV-2/2-hSyn1-dlox-hM3D(Gq)_mCherry(rev)-dlox-WPRE-hGHp(A) (AAV.flex.hM3Dq-mCherry; 7.65 x 10^8 GC)	Viral Vector Facility, University of Zurich, Switzerland	Cat#: v89-2
ssAAV-2/2-hSyn1-dlox-EGFP(rev)-dlox-WPRE-hGHp(A) (AAV.flex.eGFP; 2 x 10^8 GC)	Viral Vector Facility, University of Zurich, Switzerland	Cat#: v115-2
pssAAV-2-hSyn1-chI-dlox-EGFP_2A_FLAG_TeTxLC(rev)-dlox-WPRE-SV40p(A) (AAV.flex.TeLC.eGFP; 2 x 10^8 GC)	Viral Vector Facility, University of Zurich, Switzerland	Cat#: v322-2
ssAAV-8/2-hSyn1-dFRT-mCherry(rev)-dFRT-WPRE-hGHp(A) (AAV.FRT.mCherry; 8.7 x 10^8 GC)	Viral Vector Facility, University of Zurich, Switzerland	Cat#: v188-8
AAV9-EF1a-BbChT (AAV-Brainbow2; 1.5 - 5.96 x 10^7 GC)	Addgene, MA, USA; Deposited by Dawen Cai & Joshua Sanes	Cat#: 45186-AAV9 RRID: Addgene_45186 Cai et al. (2013), Nat Methods 10, 540-547
Antibodies		
Goat anti-Calretinin (1:1000)	SWANT, Bellinoza, Switzerland	Cat#: CG1 RRID: AB_10000342
Goat anti-cFOS (1:2000)	Santa Cruz Biotechnology Inc., CA, USA	Cat#: sc-52-G RRID: AB_2629503
Rabbit anti-DynorphinB (1:500)	Dr.Philippe Ciofi, INSERM, France	Cat#: IS-35 RRID: AB_2819033
Rabbit anti-Galanin (1:1000)	Peninsula Laboratories, CA, USA	Cat#: T-4334 RRID: AB_518348
Mouse anti-Gephyrin (1:500)	SynapticSystems, Göttingen, Germany	Cat#: 147021 RRID: AB_2232546
Chicken anti-GFP (1:1000)	Abcam plc., Cambridge, UK	Cat#: ab13970 RRID: AB_300798
Chicken anti-mCherry (1:10,000)	Abcam plc., Cambridge, UK	Cat#: ab205402 RRID: AB_2722769
Rat anti-mCherry (1:1000)	Invitrogen; Thermo Fisher Scientific, UK	Cat#: M11217 RRID: AB_2536611
Rat anti-mTFP (1:500)	Kerafast Inc., Boston, MA, USA	Cat#: EMU108
Chicken anti-NeuN (1:1000)	SynapticSystems, Göttingen, Germany	Cat#: 266006 RRID: AB_2571734
Guinea pig anti-NeuN (1:500)	SynapticSystems, Göttingen, Germany	Cat#: 266004 RRID: AB_2619988
Rabbit anti-nNOS (1:2000)	MilliporeSigma, MA, USA	Cat#: 07-571 RRID: AB_310722
Rabbit anti-NPY (1:1000)	Peninsula Laboratories, CA, USA	Cat#: T-4070 RRID: AB_518504
Guinea pig anti-Parvalbumin (1:2500)	Frontier Institute Co. Ltd, Hokkaido, Japan	Cat#: PV-GP-Af1000 RRID: AB_2336938

Rabbit anti-PAX2 (1:1000)	Invitrogen; Thermo Fisher Scientific, UK	Cat#: 71-6000 RRID: AB_2533990
Rabbit anti-PAX2 (1:200)	MilliporeSigma, MA, USA	Cat#: HPA047704 RRID: AB_2636861
Goat anti-VGAT (1:1000)	Frontier Institute Co. Ltd, Hokkaido, Japan	Cat#: VGAT-Go-Af620 RRID: AB_2571623
Alexa Fluor® 488 Donkey Anti-Chicken IgY (1:500)	Jackson ImmunoResearch, PA, USA	Cat#: 703-545-155 RRID: AB_2340375
Alexa Fluor® 488 Donkey Anti-Goat IgG (1:500)	Jackson ImmunoResearch, PA, USA	Cat#: 705-545-003 RRID: AB_2340428
Alexa Fluor® 488 Donkey Anti-Rabbit IgG (1:500)	Jackson ImmunoResearch, PA, USA	Cat#: 711-545-152 RRID: AB_2313584
Alexa Fluor® 647 Donkey Anti-Chicken IgY (1:500)	Jackson ImmunoResearch, PA, USA	Cat#: 703-605-155 RRID: AB_2340379
Alexa Fluor® 647 Donkey Anti-Goat IgG (1:500)	Jackson ImmunoResearch, PA, USA	Cat#: 705-605-147 RRID: AB_2340437
Alexa Fluor® 647 Donkey Anti-Guinea pig IgG (1:500)	Jackson ImmunoResearch, PA, USA	Cat#: 706-605-148 RRID: AB_2340476
Alexa Fluor® 647 Donkey Anti-Rabbit IgG (1:500)	Jackson ImmunoResearch, PA, USA	Cat#: 711-605-152 RRID: AB_2492288
Biotin-SP Donkey Anti-Goat IgG (1:500)	Jackson ImmunoResearch, PA, USA	Cat#: 705-065-147 RRID: AB_2340397
Biotin-SP Donkey Anti-Guinea pig IgG (1:500)	Jackson ImmunoResearch, PA, USA	Cat#: 706-065-148 RRID: AB_2340451
Biotin-SP Donkey Anti-Rabbit IgG (1:500)	Jackson ImmunoResearch, PA, USA	Cat#: 711-065-152 RRID: AB_2340593
Biotin-SP Donkey Anti-Rat IgG (1:500)	Jackson ImmunoResearch, PA, USA	Cat#: 712-065-153 RRID: AB_2315779
Rhodamine Red™-X Donkey Anti-Chicken IgY (1:100)	Jackson ImmunoResearch, PA, USA	Cat#: 703-295-155 RRID: AB_2340371
Rhodamine Red™-X Donkey Anti-Guinea pig IgG (1:100)	Jackson ImmunoResearch, PA, USA	Cat#: 706-295-148 RRID: AB_2340468
Rhodamine Red™-X Donkey Anti-Mouse IgG (1:100)	Jackson ImmunoResearch, PA, USA	Cat#: 715-295-151 RRID: AB_2340832
Rhodamine Red™-X Donkey Anti-Rabbit IgG (1:100)	Jackson ImmunoResearch, PA, USA	Cat#: 711-295-152 RRID: AB_2340613
Rhodamine Red™-X Donkey Anti-Rat IgG (1:100)	Jackson ImmunoResearch, PA, USA	Cat#: 712-295-153 RRID: AB_2340676
RNAScope probes		
Mm-Npy-C3	ACD BioTechne, CA, USA	Cat#: 313321-C3
Cre-C2	ACD BioTechne, CA, USA	Cat#: 312281-C2
Chemicals, peptides and recombinant proteins		
Clozapine-N-oxide (CNO)	Tocris, Abingdon, UK	Cat#: 4936
CNO-dihydrochloride	Tocris, Abingdon, UK	Cat#: 6329
SR95531 (Gabazine)	Abcam, Cambridge, UK	Cat#: ab120042
Strychnine hydrochloride	Sigma-Aldrich, Glasgow, UK	Cat#: S8753
Tetrodotoxin citrate (TTX)	Alamone Labs, Jerusalem, Israel	Cat#: T-550

Click here to enter text.

NBQX disodium salt	Abcam, Cambridge, UK	Cat#: ab120046
D-APV	Tocris, Abingdon, UK	Cat#: 0106
4-aminopyridine (4-AP)	Sigma-Aldrich, Glasgow, UK	Cat#: 275875
BMS 139885	Tocris, Abingdon, UK	Cat#: 3242
(-)-Bicuculline methobromide	Tocris, Abingdon, UK	Cat#: 0109
[Leu31,Pro34]-neuropeptide Y	Tocris, Abingdon, UK	Cat#: 1176
Chloroquine diphosphate salt	Sigma-Aldrich, Glasgow, UK	Cat#: C6628
Complete Freund's Adjuvant (CFA)	Sigma-Aldrich, Glasgow, UK	Cat#: F5881
Software		
Neurolucida	MBF Bioscience, VT, USA	https://www.mbfbioscience.com/neurolucida RRID: SCR_001775
Neurolucida Explorer	MBF Bioscience, VT, USA	https://www.mbfbioscience.com/neurolucida-explorer RRID: SCR_017348
pClamp	Molecular Devices, CA, USA	https://www.moleculardevices.com/products/axon-patch-clamp-system/acquisition-and-analysis-software/pclamp-software-suite#gref RRID: SCR_011323
Zen Black	Carl Zeiss, Germany	https://www.zeiss.com/microscopy/int/products/microscope-software/zen.html RRID: SCR_018163
Prism	GraphPad Software, CA, USA	https://www.graphpad.com/scientific-software/prism/ RRID: SCR_002798
Behavioral Observation Research Interactive Software (BORIS)	Oliver Friard & Marco Gamba, University of Torino, Italy	https://www.boris.unito.it/

637

638

639 **Experimental Model and Subject Details**

640 All experiments were approved by the Ethical Review Process Applications Panel
641 of the University of Glasgow, and were carried out in accordance with the European
642 Community directive 86/609/EC, the UK Animals (Scientific Procedures) Act 1986
643 and ARRIVE guidelines. The following transgenic mouse lines were utilised in this
644 study: the GENSAT BAC transgenic RH26 NPY::Cre line, which express Cre
645 recombinase under control of the NPY promoter[64]; the Ai9 Cre reporter line, in which
646 a loxP-flanked STOP cassette prevents CAG promoter-driven transcription of
647 tdTomato; the GRPR^{CreERT2} line, in which 2A-linked optimized Cre recombinase
648 fused with the ligand-binding domain of the estrogen receptor is inserted into the
649 3'UTR of the *Grpr* gene[65]; the GRPR^{FlpO} line, in which 2A-linked FlpO recombinase is
650 fused with the last exon of the *Grpr* gene[22]; and the Pdyn^{Cre} line, in which an IRES

Click here to enter text.

site fused to Cre recombinase is inserted downstream of the stop codon of the *Pdyn* gene[66]. Further details of these lines can be found in the Key Resources table. NPY::Cre and Ai9, NPY::Cre and GRPR^{CreERT2}, NPY::Cre and GRPR^{FlpO} or GRPR^{CreERT2} and Ai9 mice were crossed to produce NPY::Cre;Ai9, NPY::Cre;GRPR^{CreERT2}, NPY::Cre;GRPR^{FlpO} and GRPR^{CreERT2};Ai9 experimental animals, respectively. For experiments inolving the GRPR^{CreERT2} line, mice received 6 mg of tamoxifen (2x i.p. injections of 3 mg on consecutive days). For the NPY::Cre;GRPR^{CreERT2} mice, this was administered on the day of surgery and on the next day. Wildtype C57BL/6 mice were used for assessment of possible off-target effects of systemic CNO administration, and also to test for Cre-independent effects following injection of AAV.flex.TeLC.eGFP. Mice weighed 15 g to 28 g and animals of both sexes were used, with care taken to include approximately equal numbers of males and females. The animals were between 5 and 14 weeks old at the time of tissue harvest (for anatomy), electrophysiological recording, or behavioural testing. Where drug treatment was given (except for CPP experiments), the treatment type, or the order in which mice received the drug or vehicle was randomised. For TeLC experiments, the viral construct used for each animal was randomised. In all of these cases, the experimenter was blind to the treatment or the viral construct used.

Intraspinal AAV injections

Mice were anaesthetised with 1% to 2% isoflurane and placed in a stereotaxic frame. The skin was incised in the midline over the upper back and superficial muscle was removed from the vertebral column at the level of the T12 to L1 vertebrae, which were then clamped. The L3 and L5 spinal segments were injected through the T12/T13 and T13/L1 intervertebral spaces, respectively, whereas the L4 segment was injected via a hole drilled through the lamina of the T13 vertebra. Injections were performed by making a small slit in the dura and inserting a glass micropipette (outer/inner tip diameter: 60/40 μm) attached to a 10 μL Hamilton syringe, 400 μm lateral to the midline and 300 μm below the pial surface. The following AAV constructs were used: AAV.flex.eGFP (1.72 x 10^9 GC), AAV.flex.tdTomato (1.76 x 10^9 GC) and AAV.flex.ChR2-eYFP (5.09 x 10^8 GC), all from Penn Vector Core, PA, USA; AAV.flex.hM3Dq-mCherry, University of North Carolina Vector Core, NC, USA or University of Zurich Viral Vector Facility,

684 Switzerland, (3.8 x 10^8 or 7.65 x 10^8 GC, respectively); AAV.flex.eGFP (2 x 10^8 GC),
685 AAV.flex.TeLC.eGFP (2 x 10^8 GC) and AAV.FRT.mCherry, (8.7 x 10^8 GC), all from
686 University of Zurich Viral Vector Facility, Switzerland; and AAV-Brainbow2 (1.5 - 5.96
687 x 10^7 GC), Addgene, MA, USA. Further details of the viruses used can be found in
688 the Key Resources table. 300 nL of virus was infused per injection site (or 500nl for
689 AAV-Brainbow2) at a rate of 30-40 nL/minute using a syringe pump (Harvard
690 Apparatus, MA, USA). Pipettes were left within the spinal cord for 5 mins to minimise
691 leakage of injectate. Once injections were complete the wound was closed and
692 animals recovered with appropriate analgesic administration (0.3 mg/kg
693 buprenorphine and 5 mg/kg carprofen). The success of spinal AAV injections was
694 assessed by *post-hoc* immunohistochemical staining for the appropriate fluorescent
695 marker protein. Mice were only included for behavioural analyses if the AAV
696 injection(s) into the spinal segments relevant to the dermatome(s) being tested were
697 successful (L4 and L5 for plantar hindpaw-directed tests, L3 for calf skin-directed
698 tests; see below). In some experiments NPY::Cre;GRPR^{CreERT2} mice were injected
699 with AAV.flex.eGFP or AAV.flex.TeLC.eGFP, which should result in both NPY-
700 expressing and GRPR-expressing virus-infected cells being labelled with eGFP. This
701 was confirmed for each injection site in each animal by two methods: 1) by
702 assessing the distribution of eGFP-labelled cells, as NPY-INs are located throughout
703 laminae I-III, whereas GRPR-INs are almost entirely restricted to laminae I and IIo,
704 and 2) by antibody co-staining for the inhibitory marker Pax2, as NPY-INs in laminae
705 I-III are exclusively inhibitory, whereas GRPR-INs in laminae I and IIo are exclusively
706 excitatory. Post-AAV-injection behavioural testing was performed within 1-5 weeks
707 for experiments using AAV.flex.hM3Dq-mCherry, and within 4-6 days for
708 experiments using AAV.flex.TeLC.eGFP. For anatomical analyses of inhibitory
709 synaptic input on to GRPR-INs AAV-Brainbow2 injections were performed
710 unilaterally into the L3 and L5 segments and mice were perfused 2–3 weeks post-
711 surgery. For electrophysiological studies, AAV.flex.ChR2-eYFP, on some occasions
712 combined with AAV.FRT.mCherry, was injected unilaterally or bilaterally into the L3
713 and/or L5 segments and spinal cord slices were prepared from the mice 1–3 weeks
714 post-surgery.
715
716 **Intraplantar complete Freund's adjuvant (CFA) injections**

717 Mice were briefly anaesthetised with 1% to 2% isoflurane, the plantar surface of
718 the hindpaw ipsilateral to the spinal AAV injection was wiped with 70% ethanol and
719 20 µl of 1 mg/ml CFA was injected subcutaneously. Behavioural testing was
720 performed prior to (pre-CFA baseline) and 2 days following CFA injections.
721
722 **Spared nerve injury (SNI) surgery**
723 Mice were anaesthetised with 1% to 2% isoflurane, an incision was made in the
724 skin over the thigh ipsilateral to the spinal AAV injection and the underlying muscle
725 was blunt-dissected to reveal the sciatic nerve. The tibial and common peroneal
726 branches were identified, and 7-0 Mersilk (Ethicon, Puerto Rico) was used to apply
727 two tight ligatures 2-3 mm apart on each nerve branch. The length of nerve between
728 the ligatures was then removed and the wound was closed. Great care was taken to
729 avoid damage to the sural branch of the sciatic nerve during the surgery.
730 Behavioural testing was performed prior to (pre-SNI baseline) and from 2-4 weeks
731 following SNI surgery.
732
733 **Drug administration**
734 Clozapine-N-Oxide (CNO; Tocris Bioscience, Bristol, UK) dissolved in a 10%
735 DMSO / 90% sterile saline mixture was injected intraperitoneally (i.p.) at a dose of 5
736 mg/kg; 10% DMSO / 90% sterile saline mixture alone was used as a vehicle control.
737 In some cases we used CNO-dihydrochloride (Tocris Bioscience), dissolved in 10%
738 water / 90% sterile saline at a dose of 5 mg/kg, with 10% water / 90% sterile saline
739 as a vehicle control. For some experiments the Y1 antagonist BMS 193885 (Bio-
740 Techne, Abingdon, UK) dissolved in a 40% PEG-400 / 60% sterile saline mixture
741 was co-injected i.p. at a dose of 10 mg/kg with CNO; co-injection of the respective
742 vehicles for CNO and BMS 193885 was used as a control.
743
744 **Behavioural testing**
745 *von Frey test (noxious punctate mechanical sensitivity)*
746 Mice were placed in a plastic enclosure with mesh flooring and allowed to
747 acclimatise for at least 45 minutes. von Frey filaments of logarithmically incremental
748 stiffness (range 0.01 g to 4 g) were applied to the plantar surface of the hindpaw and
749 the 50% mechanical withdrawal threshold (MWT) was determined using Dixon's up-

750 down method[67,68]. Briefly, filaments were applied sequentially, beginning with the
751 mid-range filament (0.4 g), and the presence or absence of a withdrawal response
752 (lifting and/or shaking of the paw) was noted. If a withdrawal response was
753 observed, the next lowest filament was used subsequently; if no response was
754 observed, the next highest filament was used subsequently. Testing continued until a
755 series of six filaments had been applied from the point when the response threshold
756 was first crossed, and the 50% MWT was calculated using the formula 50% MWT =
757 $(10^{[Xf+k\delta]})/10{,}000$, where *Xf* = log value of the final filament applied, *k* = tabular value
758 (taken from Chaplan et al.[67]) based on the pattern of six positive/negative responses
759 and δ = mean difference (in log units) of the range of filaments used (0.323). When
760 testing mice that had undergone spared nerve injury, care was taken to apply von
761 Frey filaments to the sural territory of the hindpaw.
762
763 *Hargreaves test (noxious heat sensitivity)*
764 Mice were placed in plastic enclosures on a raised glass platform warmed to 25ºC
765 and allowed to acclimatise for at least 30 minutes. A radiant heat source (IITC, CA,
766 USA) set to 25% active intensity was targeted to the plantar surface of the hindpaw
767 to be tested (using an angled mirror and guide light), and the time until paw
768 withdrawal from the heat source (withdrawal latency) was noted. Testing of ipsilateral
769 and contralateral paws was alternated with at least 3 minutes interval between
770 consecutive tests, and a cut-off time of 25s was used to prevent tissue damage.
771 Each hindpaw was tested 5 times, and the average withdrawal latency calculated.
772 When testing mice that had undergone spared nerve injury, care was taken to target
773 the heat source to the sural territory of the hindpaw.
774
775 *Dry ice test (noxious cold sensitivity)*
776 Mice were placed in plastic enclosures on a raised 5 mm-thick glass platform at
777 room temperature and allowed to acclimatise for at least 45 minutes. A dry ice pellet
778 of ~1 cm diameter was applied to the underside of the glass directly below the
779 hindpaw to be tested, and the withdrawal latency was recorded[69]. Care was taken to
780 ensure that the plantar surface of the hindpaw was in direct contact with the glass
781 prior to testing. Testing of ipsilateral and contralateral paws was alternated with at
782 least 3 minutes interval between consecutive tests, and a cut-off time of 25 s was

783 used to prevent tissue damage. Each hindpaw was tested 5 times, and the average
784 withdrawal latency calculated.
785
786 *Acetone evaporation test (noxious cold sensitivity)*
787 Mice were placed in plastic enclosure with mesh flooring and allowed to
788 acclimatise for at least 30 minutes. A 10 µl droplet of acetone was applied to the
789 sural territory of the plantar hindpaw and the total amount of time spent shaking,
790 lifting and licking the paw within 30 seconds of acetone application was recorded
791 using a stopwatch. Each hindpaw was tested 3 times, with at least 3 minutes interval
792 between consecutive tests, and the average total response time calculated.
793
794 *Rotarod test (motor co-ordination)*
795 Mice were placed into the rotarod apparatus (IITC, CA, USA), which was
796 programmed to accelerate from 4 to 40 rpm over 5 minutes. Mice were allowed two
797 trial runs prior to performing four test runs, and the average maximum rpm attained
798 was calculated from the test runs.
799
800 *Pruritogen-evoked itch test*
801 Mice were acclimatised for 30 mins in plastic enclosures surrounded by angled
802 mirrors to provide unobstructed views of the targeted hindlimb, and were then video
803 recorded for 30 mins (pre-CQ). They then received 10 µl of 1% chloroquine (CQ)
804 dissolved in PBS via intradermal injection into the calf ipsilateral to the spinal AAV
805 injection (which had been shaved 24 hours prior to testing). Successful intradermal
806 injection of CQ was assessed by the appearance of a skin bleb at the injection site.
807 Mice were video recorded for 30 minutes following CQ injection (post-CQ). The
808 amount of time spent biting the injected area was scored offline either manually with
809 a stopwatch or using BORIS event logging software (freely available,
810 https://www.boris.unito.it/)[70]. Videos were viewed at one-quarter speed for analysis.
811
812 *Conditioned place preference (CPP) test*
813 To test for ongoing neuropathic pain, a three-day conditioning protocol using a
814 biased chamber assignment was used for conditioned place preference (CPP)
815 testing as described previously[71]. The custom 3-chamber CPP apparatus consisted

816 of two conditioning side chambers (170 x 150 mm) connected by a centre chamber
817 (70 x 75 mm), 180 mm tall, with infrared-transparent plastic lids (QD Plastics,
818 Dumbarton, UK). Mice were able to discriminate between chambers using visual
819 (vertical versus horizontal black-and-white striped walls) and sensory (rough versus
820 smooth textured floor) cues. On day 1 (acclimation, 7 days after SNI surgery), mice
821 had free access to explore all chambers for 30 minutes. On days 2 and 3
822 (preconditioning), mice were again allowed to freely explore for 30 min whilst their
823 position was recorded using an infrared camera and AnyMaze 7.16 software
824 (Stoelting, USA). To avoid pre-existing chamber bias, mice spending more than 90%
825 or less than 5% of time in either side chamber during preconditioning were excluded
826 (1 mouse from each experimental group). For conditioning (days 4 to 6), each
827 morning, mice received i.p. vehicle injection, were returned to their home cage for 5
828 min, then confined to their preferred side chamber for 30 min. Four hours later, mice
829 received i.p. CNO or gabapentin (100 mg/kg), were returned to their home cage for 5
830 min, and then placed in their non-preferred chamber for 30 min. On test day (day 7),
831 mice could freely explore all chambers whilst their position was recorded, as during
832 pre-conditioning, for 30 min. Difference scores were calculated as the time spent in
833 each chamber on test day minus the mean time spent during pre-conditioning.
834
835 **Noxious heat and pruritic induction of Fos**
836 Mice were injected i.p. with CNO or vehicle 30 minutes prior to receiving a noxious
837 heat or pruritic stimulation under brief isoflurane anaesthesia, ipsilateral to spinal
838 AAV.flex.hM3Dq-mCherry injection. The noxious heat stimulus was immersion of the
839 hindpaw into 52ºC water for 15 s. The pruritic stimulus was intradermal injection of
840 CQ into the calf as described above, following shaving of the leg 24 hours prior to
841 CQ injection. These mice were fitted with Elizabethan collars to prevent Fos
842 induction through scratching and/or biting of the injected area. Mice were
843 transcardially perfused under deep terminal anaesthesia 2 hours after stimulation,
844 and spinal cord tissue was processed for imaging and analysis as described below.
845
846 **Electrophysiology**
847 Electrophysiological studies were performed on spinal cord slices from NPY::Cre
848 or NPY::Cre;GRPR^{FlpO} mice that had received an intraspinal injection of

849 AAV.flex.ChR2-eYFP or AAV.flex.ChR2-eYFP combined with AAV.FRT.mCherry,
850 respectively, 1 to 3 weeks prior to recordings. Additional recordings were performed
851 on spinal cord slices from GRPR^{CreERT2};Ai9 mice. Recordings were made from 51
852 cells (39 from female, 12 from male mice) from spinal cord slices obtained from 21
853 NPY::Cre mice (16 female, 5 male) and an additional 11 cells from 5 female
854 NPY::Cre;GRPR^{FlpO} mice and 10 cells from 5 female GRPR^{CreERT2};Ai9 mice, that
855 were aged 5 to 11 weeks. Spinal cord slices were prepared as described
856 previously[72]. Mice were decapitated under isoflurane anaesthesia and the spinal
857 cord removed in ice-cold dissection solution. In some cases decapitation was
858 performed following transcardial perfusion with ice-cold dissection solution under
859 terminal anaesthesia with pentobarbital (20 mg i.p.). The lumbar region was
860 embedded in an agarose block and 300 μm parasagittal or 350 μm transverse slices
861 were cut with a vibrating blade microtome (Thermo Scientific Microm HM 650V,
862 Loughborough, UK; Leica VT1200s, Milton Keynes, UK; or Campden Instruments
863 7000smz-2, Loughborough, UK). Slices were then allowed to recover for at least 30
864 minutes in recording solution at room temperature. In some cases slices were placed
865 in an N-methyl-D-glucamine (NMDG)-based recovery solution at ~32°C for 15
866 minutes[73] before being placed in a modified recording solution at room temperature
867 for at least 30 minutes. The solutions used contained the following (in mM);
868 dissection, 251.6 sucrose, 3.0 KCl, 1.2 NaH_2PO_4, 0.5 $CaCl_2$, 7.0 $MgCl_2$, 26.0
869 $NaHCO_3$, 15.0 glucose; NMDG recovery, 93.0 NMDG, 2.5 KCl, 1.2 NaH_2PO_4, 0.5
870 $CaCl_2$, 10.0 $MgSO_4$, 30.0 $NaHCO_3$, 25.0 glucose, 5.0 Na-ascorbate, 2.0 thiourea, 3.0
871 Na-pyruvate, and 20.0 HEPES; modified recording, 92.0 NaCl, 2.5 KCl, 1.2
872 NaH_2PO_4, 2.0 $CaCl_2$, 2.0 $MgSO_4$, 30.0 $NaHCO_3$, 25.0 glucose, 5.0 Na-ascorbate, 2.0
873 thiourea, 3.0 Na-pyruvate, and 20.0 HEPES; and recording, 125.8 NaCl, 3.0 KCl, 1.2
874 NaH_2PO_4, 2.4 $CaCl_2$, 1.3 $MgCl_2$, 26.0 $NaHCO_3$, 15.0 glucose. All solutions were
875 bubbled with 95% O_2 / 5% CO_2.
876
877 Whole-cell patch-clamp recordings were made from ChR2-eYFP+ or ChR2-eYFP-
878 neurons in NPY::Cre tissue, from mCherry+ cells in NPY::Cre;GRPR^{FlpO} tissue, or
879 from tdTom+ cells in GRPR^{CreERT2};Ai9 tissue in the superficial dorsal horn, using
880 patch pipettes that had a typical resistance of 3 – 7 MΩ. Data were recorded and

881 acquired with a Multiclamp 700B amplifier and pClamp 10 software (both Molecular
882 Devices, Wokingham, UK), and were filtered at 4 kHz and digitised at 10 kHz.
883
884 To validate the optogenetic activation of NPY neurons, recordings were made
885 from ChR2-eYFP+ cells using a K-based intracellular solution. The presence of
886 optogenetically-activated currents were observed in voltage clamp mode, from a
887 holding potential of -70 mV, by illuminating the slice with brief (1 – 4 ms) pulses of
888 blue light, generated by a 470 nm LED (CoolLED pE-100, Andover, UK) and
889 delivered via the microscope objective. The ability to optogenetically drive action
890 potential firing in NPY neurons was similarly tested by applying brief pulses of blue
891 light while the membrane potential was held around -60 mV in current clamp mode.
892 Inhibition from NPY cells to other cells in the superficial dorsal horn was
893 investigated in tissue from NPY::Cre mice, by recording from ChR2-eYFP-negative
894 cells that were within the region of the viral injection, as determined by eYFP
895 expression, and applying pulses of blue light as detailed above. Inhibition of GRPR
896 cells by NPY cells was similarly assessed by recording from mCherry+ GRPR cells
897 in slices from NPY::Cre;GRPR^{FlpO} mice. Cells were classed as receiving
898 optogenetically-evoked IPSCs (oIPSCs) if there was a clear reliably evoked inward
899 current (CsCl-based intracellular, V_{hold} -70 mV), or outward current (K-based
900 intracellular, V_{hold} -40 mV; Cs-methanesulfonate-based intracellular, V_{hold} 0mV), that
901 was time-locked to the light pulse. In a subset of recordings, using CsCl-based
902 intracellular solution (V_{hold} -70 mV), the optogenetically-evoked postsynaptic currents
903 were confirmed to be non-glutamatergic by bath application of NBQX (10 μM) and D-
904 APV (30 μM). The nature of the oIPSCs recorded in unlabelled (CsCl-based
905 intracellular, V_{hold} -70 mV) and GRPR (Cs-methanesulfonate-based intracellular, V_{hold}
906 0mV) cells was investigated by bath application of the GABA antagonist, gabazine
907 (300 nM) and the glycine antagonist, strychnine (300 nM); in the case of unlabelled
908 cells this was done in the presence of NBQX and D-APV. oIPSCs were evoked 6
909 times (0.05 Hz) (Baseline) prior to the application of gabazine or strychnine, which
910 was added to the recording solution and washed into the recording chamber for 5
911 minutes before and during the recording of a further 6 oIPSCs. Strychnine was then
912 added to gabazine or gabazine added to strychnine and following a further 5 minute
913 wash in period 6 oIPSCs were recorded. oIPSCs were classified as ‘sensitive’ to

914 gabazine and/or strychnine if the drug reduced the mean peak amplitude of the
915 oIPSC to a level that was less than 2 SD of the mean peak amplitude recorded
916 during baseline or the previous drug application, and 'insensitive' if this threshold
917 was not met. The monosynaptic nature of the oIPSCs was tested in a subset of
918 GRPR cells, by investigating whether oIPSCs that were abolished by the application
919 of tetrodotoxin (TTX; 0.5 μM) could be rescued by the addition of 4-aminopyridine (4-
920 AP; 100 μM)[74]. To test whether the release of NPY from NPY cells may contribute to
921 the inhibition of GRPR cells, patch clamp recordings were made from tdTom+ GRPR
922 cells from $GRPR^{CreERT2}$;Ai9 mice to assess responses to the NPY Y_1 receptor
923 agonist, [Leu^{31},Pro^{34}]-Neuropeptide Y (300 nM), which was bath applied in the
924 presence of TTX (0.5 μM), bicuculline (10 μM) and strychnine (1 μM) (K-based
925 intracellular, V_{hold} -50 mV). Following a 1 minute baseline period, [Leu^{31},Pro^{34}]-
926 Neuropeptide Y was applied for 4 minutes, and cells where classified as responders
927 if [Leu^{31},Pro^{34}]-Neuropeptide Y resulted in an outward current of 5 pA or greater and
928 were classified as non-responders if this threshold was not reached.
929
930 The intracellular solutions used contained the following (in mM); K-based, 130.0
931 K-gluconate, 10.0 KCl, 2.0 MgCl2, 10.0 HEPES, 0.5 EGTA, 2.0 ATP-Na2, 0.5 GTP-
932 Na, and 0.2% Neurobiotin, pH adjusted to 7.3 with 1.0M KOH; CsCl-based, 130.0
933 CsCl, 1.0 MgCl2, 10.0 HEPES, 10.0 EGTA, 5.0 N-(2,6-
934 dimethylphenylcarbamoylmethyl) triethylammonium bromide (QX-314-Br), 2.0 ATP-
935 Na2, 0.3 GTP-Na, and 0.2% Neurobiotin, pH adjusted to 7.35 with 1.0M CsOH; Cs-
936 methylsulfonate-based, 120.0 Cs-methylsulfonate, 10.0 Na-methylsulfonate, 10.0
937 EGTA, 1.0 CaCl2, 10.0 HEPES, 5.0 N-(2,6-dimethylphenylcarbamoylmethyl)
938 triethylammonium chloride (QX-314-Cl), 2.0 Mg2-ATP, and 0.2% Neurobiotin, pH
939 adjusted to 7.2 with 1.0M CsOH.
940
941 All chemicals were obtained from Sigma except: TTX, QX-314-Br, QX-314-Cl
942 (Alomone, Jerusalem, Israel), Gabazine, NBQX (Abcam, Cambridge, UK), sucrose,
943 glucose, NaH_2PO_4 (VWR, Lutterworth, UK), D-APV, [Leu^{31},Pro^{34}]-Neuropeptide Y
944 (Tocris, Abingdon, UK) and Neurobiotin (Vector Labs, Peterborough, UK).
945
946 **Immunohistochemistry (IHC)**

947 Animals were terminally anaesthetised with pentobarbital (20 mg i.p.) and
948 transcardially perfused with 4% freshly depolymerised formaldehyde. The spinal cord
949 was then dissected out and post-fixed in the same fixative for 2 hours, and 60 μm-
950 thick transverse or sagittal sections from appropriate lumbar sections were cut on a
951 vibrating microtome. Sections were immersed in 50% ethanol for 30 minutes to
952 enhance antibody penetration before incubation in appropriate primary and
953 secondary antibodies at 4ºC for 72 and 24 hours, respectively. Details of the
954 antibodies used in this study can be found in the Key Resources table. Sections
955 were continuously agitated during antibody incubation and washed 3 times in PBS
956 that contained 0.3 M NaCl following each incubation. Following the final PBS wash,
957 sections were mounted on slides in Vectashield anti-fade mounting medium (Vector
958 Laboratories, CA, USA). In some cases lumbar dorsal root ganglia (DRGs) were also
959 removed and processed intact for IHC before whole-mounting on slides.
960

961 **Fluorescent in situ hybridisation (FISH)**

962 Multiple-labelling FISH was performed using RNAscope probes and RNAscope
963 fluorescent multiplex reagent kit 320850 (ACD BioTechne, CA, USA). Mice were
964 deeply anaesthetised, the spinal cord was rapidly removed by hydraulic extrusion
965 and the lumbar enlargement was excised and snap-frozen on dry ice. Lumbar
966 segments were then embedded in OCT mounting medium and 12 μm-thick
967 transverse sections were cut on a Leica CM 1950 cryostat (Leica, Milton Keynes,
968 UK). Sections were mounted non-sequentially (such that sections on the same slide
969 were at least 4 apart) onto SuperFrost Plus slides (VWR, Lutterworth, UK) and air-
970 dried. The slides were then reacted according to the manufacturer's recommended
971 protocol, using probes against *Cre* and *Npy* that were revealed with Atto 550 and
972 Alexa 647, respectively. Further details of the probes used can be found in the Key
973 Resources table. Sections were mounted using Prolong-Glass anti-fade medium
974 containing NucBlue (Hoescht 33342) nuclear stain (ThermoFisher Scientific, Paisley,
975 UK).
976

977 **Image acquisition and analysis**

978 IHC and FISH slides were imaged with a Zeiss LSM 710 confocal microscope
979 system equipped with Ar multi-line, 405-nm diode, 561-nm solid-state and HeNe

980 lasers. For analyses of AAV.flex.FP, AAV.flex.hM3Dq-mCherry or
981 AAV.flex.TeLC.eGFP-labelled cells image stacks were taken through a 40x objective
982 (NA = 1.3) at a z-separation of 1 μm. For assessment of spinal injection sites and
983 analysis of mCherry expression in DRGs of AAV.flex.hM3Dq-mCherry-injected mice,
984 image stacks were taken through a 10x objective (NA = 0.3) at a z-separation of 2
985 μm. Image analysis was performed using Neurolucida software (MBF Bioscience,
986 VT, USA). For comparison of tdTomato or eGFP expression with NPY
987 immunoreactivity in AAV.flex.tdTomato- or AAV.flex.eGFP-injected NPY::Cre mice,
988 and in AAV.flex.eGFP-injected NPY::Cre;Ai9 mice, a modified optical disector
989 method was used[75]. All structures labelled with the neuronal marker NeuN that had
990 their bottom surface between reference and look-up sections separated by 10 μm
991 (10 optical sections) were marked within the injection site in laminae I-III. The NPY-
992 IR, eGFP and/or tdTomato channels were then viewed separately and sequentially,
993 and the NeuN profiles were marked as positive or negative as appropriate. As NPY-
994 IR varies greatly from cell to cell and is often observed as discrete clumps within the
995 perikaryal cytoplasm[10,26], cells were classified as NPY-positive if clear above-
996 background signal was observed in at least 3 consecutive optical sections. Markers
997 from previously-assessed channels were hidden as the channels were analysed in
998 sequence, to prevent bias. The same method was used to compare mCherry, Fos
999 and Pax2 or mCherry, Fos and NPY immunoreactivity in vehicle- or CNO-dosed
1000 AAV.flex.hM3Dq-mCherry spinal-injected NPY::Cre mice, as well as eGFP and NPY
1001 immunoreactivity in AAV.flex.TeLC.eGFP spinal-injected NPY::Cre mice. A similar
1002 method was used to compare mCherry, Fos and Pax2 in the vehicle- or CNO-dosed
1003 AAV.flex.hM3Dq-mCherry spinal-injected NPY::Cre mice that received noxious heat
1004 or pruritic stimuli 2 hours prior to perfusion; however in this case the reference and
1005 look-up sections were separated by 20 μm (20 optical sections) and analyses were
1006 restricted to the somatotopically-relevant areas of laminae I and II (medial half for
1007 noxious heat stimulation of hindpaw, middle third for CQ injection into calf). For
1008 comparison of tdTomato and eGFP or mCherry expression with neurochemical
1009 markers of inhibitory interneuron populations in AAV.flex.eGFP-injected
1010 NPY::Cre;Ai9 or AAV.flex.hM3Dq-mCherry-injected NPY::Cre mice, respectively, all
1011 cells expressing the neurochemical markers and fluorescent protein(s) in laminae I
1012 and II were marked throughout the whole section thickness. Each channel was again

1013 assessed separately and sequentially, with markers from previously-assessed
1014 channels hidden to prevent bias. Only cells with the maximal profile of their soma
1015 contained within the z stack were counted. mCherry-positive cells in whole-mounted
1016 DRGs from AAV.flex.hM3Dq-mCherry-injected NPY::Cre mice that underwent SNI
1017 surgery were counted using the same method.

1018 For analysis of inhibitory synapses onto GRPR-INs, 9 mTFP-labelled cells in total
1019 were selected from tissue of 3 AAV-Brainbow2-injected GRPR^{CreERT2} mice
1020 immunostained for mTFP, VGAT, gephyrin and NPY or Dynorphin B (3 per animal
1021 for Dynorphin B and 2, 3 and 4 cells for NPY analyses). Cell selection was
1022 performed before the staining for axonal markers was visualised and was based on
1023 the completeness of dendritic labelling and separation from other nearby mTFP-
1024 labelled neurons. The selected cells were scanned through a 63x oil-immersion lens
1025 (numerical aperture 1.4) at a z-separation of 0.3 µm. Z-series were obtained from as
1026 much of the dendritic tree as was visible in the section. For analysis, the mTFP and
1027 gephyrin channels were initially viewed and the cell bodies and dendritic trees were
1028 traced based on the mTFP signal. The locations of all gephyrin puncta associated
1029 with the cell body and dendritic tree were then plotted. The VGAT channel was then
1030 viewed and the presence or absence of an apposed VGAT-immunoreactive bouton
1031 was noted for each gephyrin punctum. Finally, the remaining channel (corresponding
1032 to NPY or Dynorphin B) was revealed and the presence or absence of peptide
1033 staining was noted for each of the VGAT boutons that contacted a gephyrin punctum
1034 on the selected cell. To determine the frequency of all boutons arising from inhibitory
1035 interneurons that were positive for each of the neuropeptides, we sampled from
1036 those VGAT-immunoreactive boutons in the vicinity of the mTFP-labelled cell. A 4 x
1037 4 µm grid was applied within a box drawn to include the entire dendritic tree of the
1038 cell. Only the VGAT channel was viewed initially and in each successive grid square,
1039 the VGAT-immunoreactive bouton nearest the bottom right of the square was
1040 selected. The presence or absence of NPY or DynorphinB was then recorded for
1041 each of these selected VGAT-immunoreactive boutons.

1042 For comparison of *Cre* and *Npy* mRNA in FISH sections, all NucBlue profiles
1043 within a single optical section were marked throughout laminae I-III. The *Cre* and
1044 *Npy* channels were then viewed separately and sequentially and cells were marked
1045 as positive if they contained ≥4 labelled transcript particles. Markers from the mRNA

1046 channel that was assessed first were hidden during assessment of the second
1047 channel to prevent bias.
1048
1049 **Quantification and statistical analysis**
1050 Data are reported as mean ± SEM, unless stated otherwise. Statistical analyses
1051 were performed using Prism software (v7,v8 & v9,GraphPad Software, CA, USA).
1052 Behavioural and anatomical analyses involving drug treatments were analysed blind
1053 to treatment group. Behavioural analyses involving AAV.flex.TeLC.eGFP-mediated
1054 silencing and AAV.flex.eGFP-injected controls were analysed blind to the AAV
1055 injected. The statistical tests used for each experiment, including tests for multiple
1056 comparisons, are given in the appropriate figure legends. A p value of <0.05 was
1057 considered significant, and significance markers are denoted within figures as
1058 follows: *p < 0.05, **p < 0.01, ***p < 0.001, ****p < 0.0001.
1059
1060 **Data and materials availability**
1061 Upon acceptance of this manuscript, all data will be made accessible from the
1062 Enlighten: Research Data open repository hosted at the University of Glasgow. This
1063 study did not generate any new materials, reagents or code.
1064
1065
1066 **ACKNOWLEDGMENTS**
1067 This research was funded in whole, or in part, by the Wellcome Trust (Grant
1068 numbers 102645/Z/13/Z and 219433/Z/19/Z), the Biotechnology and Biological
1069 Sciences Research Council (Grant numbers BB/N006119/1, BB/P007996/1) and the
1070 Medical Research Council (Grant numbers MR/S002987/1, MR/T01072X/1 and
1071 MR/V033638/1). For the purpose of Open Access, the authors have applied a CC
1072 BY public copyright licence to any Author Accepted Manuscript version arising from
1073 this submission. We are grateful to R Kerr, C Watt and I Plenderleith for expert
1074 technical assistance, to Yan-Gang Sun for the gift of GRPR^{CrERT2} and GRPR^{FlpO}
1075 mice, to Dr Philippe Ciofi for the Dynorphin B antibody and to Dr Mark Hoon for
1076 helpful discussion.
1077
1078

AUTHOR CONTRIBUTIONS

K.A.B., E.P., M.G.-M., A.C.D., A.H.C., A.M.B., G.A.W., J.S.R. and A.J.T. conceived the project and designed experiments. A.J.T. and J.S.R. obtained funding. K.A.B., E.P., M.G.-M., A.C.D., A.H.C., A.M.B. and D.I.H. performed experiments. K.A.B., E.P., M.G.-M., A.C.D., A.H.C., A.M.B., M.E.J. and A.C.-B. analysed data. M.W. provided reagents. K.A.B., A.C.D., A.H.C., A.M.B., G.A.W. and A.J.T. wrote the paper. All of the authors provided feedback and contributed to editing of the manuscript.

COMPETING INTERESTS

The authors declare no competing interests.

REFERENCES

1. Abraira, V.E., and Ginty, D.D. (2013). The sensory neurons of touch. Neuron *79*, 618-639. 10.1016/j.neuron.2013.07.051.
2. Todd, A.J. (2010). Neuronal circuitry for pain processing in the dorsal horn. Nature reviews. Neuroscience *11*, 823-836. 10.1038/nrn2947.
3. Mishra, S.K., and Hoon, M.A. (2015). Transmission of pruriceptive signals. Handbook of experimental pharmacology *226*, 151-162. 10.1007/978-3-662-44605-8_8.
4. Braz, J., Solorzano, C., Wang, X., and Basbaum, A.I. (2014). Transmitting pain and itch messages: a contemporary view of the spinal cord circuits that generate gate control. Neuron *82*, 522-536. 10.1016/j.neuron.2014.01.018.
5. Cevikbas, F., and Lerner, E.A. (2020). Physiology and Pathophysiology of Itch. Physiol Rev *100*, 945-982. 10.1152/physrev.00017.2019.
6. Beyer, C., Roberts, L.A., and Komisaruk, B.R. (1985). Hyperalgesia induced by altered glycinergic activity at the spinal cord. Life Sci *37*, 875-882.
7. Foster, E., Wildner, H., Tudeau, L., Haueter, S., Ralvenius, W.T., Jegen, M., Johannssen, H., Hosli, L., Haenraets, K., Ghanem, A., et al. (2015). Targeted ablation, silencing, and activation establish glycinergic dorsal horn neurons as key components of a spinal gate for pain and itch. Neuron *85*, 1289-1304. 10.1016/j.neuron.2015.02.028.
8. Sivilotti, L., and Woolf, C.J. (1994). The contribution of GABAA and glycine receptors to central sensitization: disinhibition and touch-evoked allodynia in the spinal cord. Journal of neurophysiology *72*, 169-179.
9. Yaksh, T.L. (1989). Behavioral and autonomic correlates of the tactile evoked allodynia produced by spinal glycine inhibition: effects of modulatory receptor systems and excitatory amino acid antagonists. Pain *37*, 111-123.
10. Boyle, K.A., Gutierrez-Mecinas, M., Polgar, E., Mooney, N., O'Connor, E., Furuta, T., Watanabe, M., and Todd, A.J. (2017). A quantitative study of neurochemically defined populations of inhibitory interneurons in the

Click here to enter text.

1121 superficial dorsal horn of the mouse spinal cord. Neuroscience *363*, 120-133.
1122 10.1016/j.neuroscience.2017.08.044.
1123 11. Häring, M., Zeisel, A., Hochgerner, H., Rinwa, P., Jakobsson, J.E.T.,
1124 Lonnerberg, P., La Manno, G., Sharma, N., Borgius, L., Kiehn, O., et al.
1125 (2018). Neuronal atlas of the dorsal horn defines its architecture and links
1126 sensory input to transcriptional cell types. Nature neuroscience *21*, 869-880.
1127 10.1038/s41593-018-0141-1.
1128 12. Sathyamurthy, A., Johnson, K.R., Matson, K.J.E., Dobrott, C.I., Li, L., Ryba,
1129 A.R., Bergman, T.B., Kelly, M.C., Kelley, M.W., and Levine, A.J. (2018).
1130 Massively Parallel Single Nucleus Transcriptional Profiling Defines Spinal
1131 Cord Neurons and Their Activity during Behavior. Cell Rep *22*, 2216-2225.
1132 10.1016/j.celrep.2018.02.003.
1133 13. Polgár, E., Sardella, T.C., Tiong, S.Y., Locke, S., Watanabe, M., and Todd,
1134 A.J. (2013). Functional differences between neurochemically defined
1135 populations of inhibitory interneurons in the rat spinal dorsal horn. Pain *154*,
1136 2606-2615. 10.1016/j.pain.2013.05.001.
1137 14. Boyle, K.A., Gradwell, M.A., Yasaka, T., Dickie, A.C., Polgar, E., Ganley,
1138 R.P., Orr, D.P.H., Watanabe, M., Abraira, V.E., Kuehn, E.D., et al. (2019).
1139 Defining a Spinal Microcircuit that Gates Myelinated Afferent Input:
1140 Implications for Tactile Allodynia. Cell reports *28*, 526-540 e526.
1141 10.1016/j.celrep.2019.06.040.
1142 15. Petitjean, H., Pawlowski, S.A., Fraine, S.L., Sharif, B., Hamad, D., Fatima, T.,
1143 Berg, J., Brown, C.M., Jan, L.Y., Ribeiro-da-Silva, A., et al. (2015). Dorsal
1144 horn parvalbumin neurons are gate-keepers of touch-evoked pain after nerve
1145 injury. Cell reports *13*, 1246-1257. 10.1016/j.celrep.2015.09.080.
1146 16. Huang, J., Polgar, E., Solinski, H.J., Mishra, S.K., Tseng, P.Y., Iwagaki, N.,
1147 Boyle, K.A., Dickie, A.C., Kriegbaum, M.C., Wildner, H., et al. (2018). Circuit
1148 dissection of the role of somatostatin in itch and pain. Nature neuroscience
1149 *21*, 707-716. 10.1038/s41593-018-0119-z.
1150 17. Duan, B., Cheng, L., Bourane, S., Britz, O., Padilla, C., Garcia-Campmany, L.,
1151 Krashes, M., Knowlton, W., Velasquez, T., Ren, X., et al. (2014). Identification
1152 of spinal circuits transmitting and gating mechanical pain. Cell *159*, 1417-
1153 1432. 10.1016/j.cell.2014.11.003.
1154 18. Bourane, S., Duan, B., Koch, S.C., Dalet, A., Britz, O., Garcia-Campmany, L.,
1155 Kim, E., Cheng, L., Ghosh, A., Ma, Q., and Goulding, M. (2015). Gate control
1156 of mechanical itch by a subpopulation of spinal cord interneurons. Science
1157 *350*, 550-554. 10.1126/science.aac8653.
1158 19. Koch, S.C., Acton, D., and Goulding, M. (2018). Spinal Circuits for Touch,
1159 Pain, and Itch. Annual review of physiology *80*, 189-217. 10.1146/annurev-
1160 physiol-022516-034303.
1161 20. Pan, H., Fatima, M., Li, A., Lee, H., Cai, W., Horwitz, L., Hor, C.C., Zaher, N.,
1162 Cin, M., Slade, H., et al. (2019). Identification of a Spinal Circuit for
1163 Mechanical and Persistent Spontaneous Itch. Neuron *103*, 1135-1149 e1136.
1164 10.1016/j.neuron.2019.06.016.
1165 21. Acton, D., Ren, X., Di Costanzo, S., Dalet, A., Bourane, S., Bertocchi, I., Eva,
1166 C., and Goulding, M. (2019). Spinal Neuropeptide Y1 Receptor-Expressing
1167 Neurons Form an Essential Excitatory Pathway for Mechanical Itch. Cell
1168 reports *28*, 625-639 e626. 10.1016/j.celrep.2019.06.033.
1169 22. Liu, M.Z., Chen, X.J., Liang, T.Y., Li, Q., Wang, M., Zhang, X.Y., Li, Y.Z., Sun,
1170 Q., and Sun, Y.G. (2019). Synaptic control of spinal GRPR+ neurons by local

Click here to enter text.

and long-range inhibitory inputs. Proceedings of the National Academy of Sciences of the United States of America *116*, 27011-27017. 10.1073/pnas.1905658116.

23. Chen, S., Gao, X.F., Zhou, Y., Liu, B.L., Liu, X.Y., Zhang, Y., Barry, D.M., Liu, K., Jiao, Y., Bardoni, R., et al. (2020). A spinal neural circuitry for converting touch to itch sensation. Nature communications *11*, 5074. 10.1038/s41467-020-18895-7.
24. Chen, X.J., and Sun, Y.G. (2020). Central circuit mechanisms of itch. Nature communications *11*, 3052. 10.1038/s41467-020-16859-5.
25. Cameron, D., Polgar, E., Gutierrez-Mecinas, M., Gomez-Lima, M., Watanabe, M., and Todd, A.J. (2015). The organisation of spinoparabrachial neurons in the mouse. Pain *156*, 2061-2071. 10.1097/j.pain.0000000000000270.
26. Iwagaki, N., Ganley, R.P., Dickie, A.C., Polgár, E., Hughes, D.I., Del Rio, P., Revina, Y., Watanabe, M., Todd, A.J., and Riddell, J.S. (2016). A combined electrophysiological and morphological study of neuropeptide Y-expressing inhibitory interneurons in the spinal dorsal horn of the mouse. Pain *157*, 598-612. 10.1097/j.pain.0000000000000407.
27. Kokai, E., Alsulaiman, W.A.A., Dickie, A.C., Bell, A.M., Goffin, L., Watanabe, M., Gutierrez-Mecinas, M., and Todd, A.J. (2022). Characterisation of deep dorsal horn projection neurons in the spinal cord of the Phox2a::Cre mouse line. Molecular pain *in press*.
28. Polgár, E., Sardella, T.C., Watanabe, M., and Todd, A.J. (2011). Quantitative study of NPY-expressing GABAergic neurons and axons in rat spinal dorsal horn. The Journal of comparative neurology *519*, 1007-1023. 10.1002/cne.22570.
29. Solway, B., Bose, S.C., Corder, G., Donahue, R.R., and Taylor, B.K. (2011). Tonic inhibition of chronic pain by neuropeptide Y. Proceedings of the National Academy of Sciences of the United States of America *108*, 7224-7229. 10.1073/pnas.1017719108.
30. Tashima, R., Koga, K., Yoshikawa, Y., Sekine, M., Watanabe, M., Tozaki-Saitoh, H., Furue, H., Yasaka, T., and Tsuda, M. (2021). A subset of spinal dorsal horn interneurons crucial for gating touch-evoked pain-like behavior. Proceedings of the National Academy of Sciences of the United States of America *118*. 10.1073/pnas.2021220118.
31. Larsson, M. (2017). Pax2 is persistently expressed by GABAergic neurons throughout the adult rat dorsal horn. Neuroscience letters *638*, 96-101. 10.1016/j.neulet.2016.12.015.
32. Smith, K.M., Boyle, K.A., Madden, J.F., Dickinson, S.A., Jobling, P., Callister, R.J., Hughes, D.I., and Graham, B.A. (2015). Functional heterogeneity of calretinin-expressing neurons in the mouse superficial dorsal horn: implications for spinal pain processing. The Journal of physiology *593*, 4319-4339. 10.1113/JP270855.
33. Honore, P., Rogers, S.D., Schwei, M.J., Salak-Johnson, J.L., Luger, N.M., Sabino, M.C., Clohisy, D.R., and Mantyh, P.W. (2000). Murine models of inflammatory, neuropathic and cancer pain each generates a unique set of neurochemical changes in the spinal cord and sensory neurons. Neuroscience *98*, 585-598. 10.1016/s0306-4522(00)00110-x.
34. Bell, A.M., Gutierrez-Mecinas, M., Polgar, E., and Todd, A.J. (2016). Spinal neurons that contain gastrin-releasing peptide seldom express Fos or

Click here to enter text.

phosphorylate extracellular signal-regulated kinases in response to intradermal chloroquine. Molecular pain *12*. 10.1177/1744806916649602.

35. Gutierrez-Mecinas, M., Bell, A.M., Marin, A., Taylor, R., Boyle, K.A., Furuta, T., Watanabe, M., Polgár, E., and Todd, A.J. (2017). Preprotachykinin A is expressed by a distinct population of excitatory neurons in the mouse superficial spinal dorsal horn including cells that respond to noxious and pruritic stimuli. Pain *158*, 440-456. 10.1097/j.pain.0000000000000778.

36. Rowan, S., Todd, A.J., and Spike, R.C. (1993). Evidence that neuropeptide Y is present in GABAergic neurons in the superficial dorsal horn of the rat spinal cord. Neuroscience *53*, 537-545. 0306-4522(93)90218-5 [pii].

37. Gomez, J.L., Bonaventura, J., Lesniak, W., Mathews, W.B., Sysa-Shah, P., Rodriguez, L.A., Ellis, R.J., Richie, C.T., Harvey, B.K., Dannals, R.F., et al. (2017). Chemogenetics revealed: DREADD occupancy and activation via converted clozapine. Science *357*, 503-507. 10.1126/science.aan2475.

38. Intondi, A.B., Zadina, J.E., Zhang, X., and Taylor, B.K. (2010). Topography and time course of changes in spinal neuropeptide Y immunoreactivity after spared nerve injury. Neuroscience *165*, 914-922. 10.1016/j.neuroscience.2009.10.052.

39. Wakisaka, S., Kajander, K.C., and Bennett, G.J. (1991). Increased neuropeptide Y (NPY)-like immunoreactivity in rat sensory neurons following peripheral axotomy. Neuroscience letters *124*, 200-203.

40. Wakisaka, S., Kajander, K.C., and Bennett, G.J. (1992). Effects of peripheral nerve injuries and tissue inflammation on the levels of neuropeptide Y-like immunoreactivity in rat primary afferent neurons. Brain research *598*, 349-352.

41. Duchen, L.W., and Scaravilli, F. (1977). Quantitative and electron microscopic studies of sensory ganglion cells of the Sprawling mouse. Journal of neurocytology *6*, 465-481. 10.1007/bf01178229.

42. Lawson, S.N. (1979). The postnatal development of large light and small dark neurons in mouse dorsal root ganglia: a statistical analysis of cell numbers and size. Journal of neurocytology *8*, 275-294. 10.1007/bf01236123.

43. Nelson, T.S., Fu, W., Donahue, R.R., Corder, G.F., Hokfelt, T., Wiley, R.G., and Taylor, B.K. (2019). Facilitation of neuropathic pain by the NPY Y1 receptor-expressing subpopulation of excitatory interneurons in the dorsal horn. Scientific reports *9*, 7248. 10.1038/s41598-019-43493-z.

44. Nelson, T.S., Sinha, G.P., Santos, D.F.S., Jukkola, P., Prasoon, P., Winter, M.K., McCarson, K.E., Smith, B.N., and Taylor, B.K. (2022). Spinal neuropeptide Y Y1 receptor-expressing neurons are a pharmacotherapeutic target for the alleviation of neuropathic pain. Proceedings of the National Academy of Sciences of the United States of America *119*, e2204515119. 10.1073/pnas.2204515119.

45. King, T., Vera-Portocarrero, L., Gutierrez, T., Vanderah, T.W., Dussor, G., Lai, J., Fields, H.L., and Porreca, F. (2009). Unmasking the tonic-aversive state in neuropathic pain. Nature neuroscience *12*, 1364-1366. 10.1038/nn.2407.

46. Mishra, S.K., and Hoon, M.A. (2013). The cells and circuitry for itch responses in mice. Science *340*, 968-971. 10.1126/science.1233765.

47. Sun, Y.G., and Chen, Z.F. (2007). A gastrin-releasing peptide receptor mediates the itch sensation in the spinal cord. Nature *448*, 700-703. nature06029 [pii] 10.1038/nature06029.

48. Sun, Y.G., Zhao, Z.Q., Meng, X.L., Yin, J., Liu, X.Y., and Chen, Z.F. (2009). Cellular basis of itch sensation. Science *325*, 1531-1534. 1174868 [pii] 10.1126/science.1174868.
49. Kardon, A.P., Polgár, E., Hachisuka, J., Snyder, L.M., Cameron, D., Savage, S., Cai, X., Karnup, S., Fan, C.R., Hemenway, G.M., et al. (2014). Dynorphin acts as a neuromodulator to inhibit itch in the dorsal horn of the spinal cord. Neuron *82*, 573-586. 10.1016/j.neuron.2014.02.046.
50. Ross, S.E., Mardinly, A.R., McCord, A.E., Zurawski, J., Cohen, S., Jung, C., Hu, L., Mok, S.I., Shah, A., Savner, E.M., et al. (2010). Loss of inhibitory interneurons in the dorsal spinal cord and elevated itch in Bhlhb5 mutant mice. Neuron *65*, 886-898. S0896-6273(10)00142-X [pii] 10.1016/j.neuron.2010.02.025.
51. Brewer, C.L., Styczynski, L.M., Serafin, E.K., and Baccei, M.L. (2020). Postnatal maturation of spinal dynorphin circuits and their role in somatosensation. Pain *161*, 1906-1924. 10.1097/j.pain.0000000000001884.
52. Zhang, X., Bao, L., Xu, Z.Q., Kopp, J., Arvidsson, U., Elde, R., and Hokfelt, T. (1994). Localization of neuropeptide Y Y1 receptors in the rat nervous system with special reference to somatic receptors on small dorsal root ganglion neurons. Proceedings of the National Academy of Sciences of the United States of America *91*, 11738-11742.
53. Nelson, T.S., and Taylor, B.K. (2021). Targeting spinal neuropeptide Y1 receptor-expressing interneurons to alleviate chronic pain and itch. Progress in neurobiology *196*, 101894. 10.1016/j.pneurobio.2020.101894.
54. Polgár, E., Dickie, A.C., Gutierrez-Mecinas, M., Bell, A.M., Boyle, K.A., Quillet, R., Ab Rashid, E., Clark, R.A., German, M.T., Watanabe, M., et al. (2022). *Grpr* expression defines a population of superficial dorsal horn vertical cells that have a role in both itch and pain. Pain *in press*.
55. Lu, Y., and Perl, E.R. (2005). Modular organization of excitatory circuits between neurons of the spinal superficial dorsal horn (laminae I and II). The Journal of neuroscience : the official journal of the Society for Neuroscience *25*, 3900-3907.
56. Lu, Y., Dong, H., Gao, Y., Gong, Y., Ren, Y., Gu, N., Zhou, S., Xia, N., Sun, Y.Y., Ji, R.R., and Xiong, L. (2013). A feed-forward spinal cord glycinergic neural circuit gates mechanical allodynia. The Journal of clinical investigation *123*, 4050-4062. 10.1172/JCI70026.
57. Peirs, C., and Seal, R.P. (2016). Neural circuits for pain: Recent advances and current views. Science *354*, 578-584. 10.1126/science.aaf8933.
58. Polgár, E., Shehab, S.A., Watt, C., and Todd, A.J. (1999). GABAergic neurons that contain neuropeptide Y selectively target cells with the neurokinin 1 receptor in laminae III and IV of the rat spinal cord. The Journal of neuroscience : the official journal of the Society for Neuroscience *19*, 2637-2646.
59. Intondi, A.B., Dahlgren, M.N., Eilers, M.A., and Taylor, B.K. (2008). Intrathecal neuropeptide Y reduces behavioral and molecular markers of inflammatory or neuropathic pain. Pain *137*, 352-365. 10.1016/j.pain.2007.09.016.
60. Miranda, C.O., Hegedus, K., Wildner, H., Zeilhofer, H.U., and Antal, M. (2022). Morphological and neurochemical characterization of glycinergic neurons in laminae I-IV of the mouse spinal dorsal horn. The Journal of comparative neurology *530*, 607-626. 10.1002/cne.25232.

61. Albisetti, G.W., Ganley, R.P., Pietrafesa, F., Werynska, K., Magalhaes de Sousa, M., Sipione, R., Scheurer, L., Bosl, M.R., Pelczar, P., Wildner, H., and Zeilhofer, H.U. (2022). Inhibitory Kcnip2 neurons of the spinal dorsal horn control behavioral sensitivity to environmental cold. Neuron. 10.1016/j.neuron.2022.10.008.
62. Yadav, A., Matson, K.J.E., Li, L., Hua, I., Petrescu, J., Kang, K., Alkaslasi, M.R., Lee, D.I., Hasan, S., Galuta, A., et al. (2022). A Cellular Taxonomy of the Adult Human Spinal Cord. BioRxiv preprint. https://doi.org/10.1101/2022.03.25.485808.
63. Baron, R., Maier, C., Attal, N., Binder, A., Bouhassira, D., Cruccu, G., Finnerup, N.B., Haanpaa, M., Hansson, P., Hullemann, P., et al. (2017). Peripheral neuropathic pain: a mechanism-related organizing principle based on sensory profiles. Pain *158*, 261-272. 10.1097/j.pain.0000000000000753.
64. Gerfen, C.R., Paletzki, R., and Heintz, N. (2013). GENSAT BAC cre-recombinase driver lines to study the functional organization of cerebral cortical and basal ganglia circuits. Neuron *80*, 1368-1383. 10.1016/j.neuron.2013.10.016.
65. Mu, D., Deng, J., Liu, K.F., Wu, Z.Y., Shi, Y.F., Guo, W.M., Mao, Q.Q., Liu, X.J., Li, H., and Sun, Y.G. (2017). A central neural circuit for itch sensation. Science *357*, 695-699. 10.1126/science.aaf4918.
66. Krashes, M.J., Shah, B.P., Madara, J.C., Olson, D.P., Strochlic, D.E., Garfield, A.S., Vong, L., Pei, H., Watabe-Uchida, M., Uchida, N., et al. (2014). An excitatory paraventricular nucleus to AgRP neuron circuit that drives hunger. Nature *507*, 238-242. 10.1038/nature12956.
67. Chaplan, S.R., Bach, F.W., Pogrel, J.W., Chung, J.M., and Yaksh, T.L. (1994). Quantitative assessment of tactile allodynia in the rat paw. Journal of neuroscience methods *53*, 55-63.
68. Dixon, W.J. (1980). Efficient analysis of experimental observations. Annu Rev Pharmacol Toxicol *20*, 441-462. 10.1146/annurev.pa.20.040180.002301.
69. Brenner, D.S., Golden, J.P., and Gereau, R.W.t. (2012). A novel behavioral assay for measuring cold sensation in mice. PloS one *7*, e39765. 10.1371/journal.pone.0039765.
70. Friard, O., and Gamba, M. (2016). BORIS: a free, versatile open-source event-logging software for video/audio coding and live observations. Methods Ecol Evol *7*, 1325-1330. 10.1111/2041-210x.12584.
71. Cooper, A.H., Hedden, N.S., Corder, G., Lamerand, S.R., Donahue, R.R., Morales-Medina, J.C., Selan, L., Prasoon, P., and Taylor, B.K. (2022). Endogenous mu-opioid receptor activity in the lateral and capsular subdivisions of the right central nucleus of the amygdala prevents chronic postoperative pain. Journal of neuroscience research *100*, 48-65. 10.1002/jnr.24846.
72. Dickie, A.C., Bell, A.M., Iwagaki, N., Polgar, E., Gutierrez-Mecinas, M., Kelly, R., Lyon, H., Turnbull, K., West, S.J., Etlin, A., et al. (2019). Morphological and functional properties distinguish the substance P and gastrin-releasing peptide subsets of excitatory interneuron in the spinal cord dorsal horn. Pain *160*, 442-462. 10.1097/j.pain.0000000000001406.
73. Ting, J.T., Daigle, T.L., Chen, Q., and Feng, G. (2014). Acute Brain Slice Methods for Adult and Aging Animals: Application of Targeted Patch Clamp Analysis and Optogenetics. In Patch-Clamp Methods and Protocols, M.

Martina, and S. Taverna, eds. (Springer New York), pp. 221-242. 10.1007/978-1-4939-1096-0_14.

74. Petreanu, L., Mao, T., Sternson, S.M., and Svoboda, K. (2009). The subcellular organization of neocortical excitatory connections. Nature *457*, 1142-1145. 10.1038/nature07709.

75. Polgár, E., Gray, S., Riddell, J.S., and Todd, A.J. (2004). Lack of evidence for significant neuronal loss in laminae I-III of the spinal dorsal horn of the rat in the chronic constriction injury model. Pain *111*, 144-150. 10.1016/j.pain.2004.06.011 S0304395904002994 [pii].

1376 **MAIN FIGURES**

1377

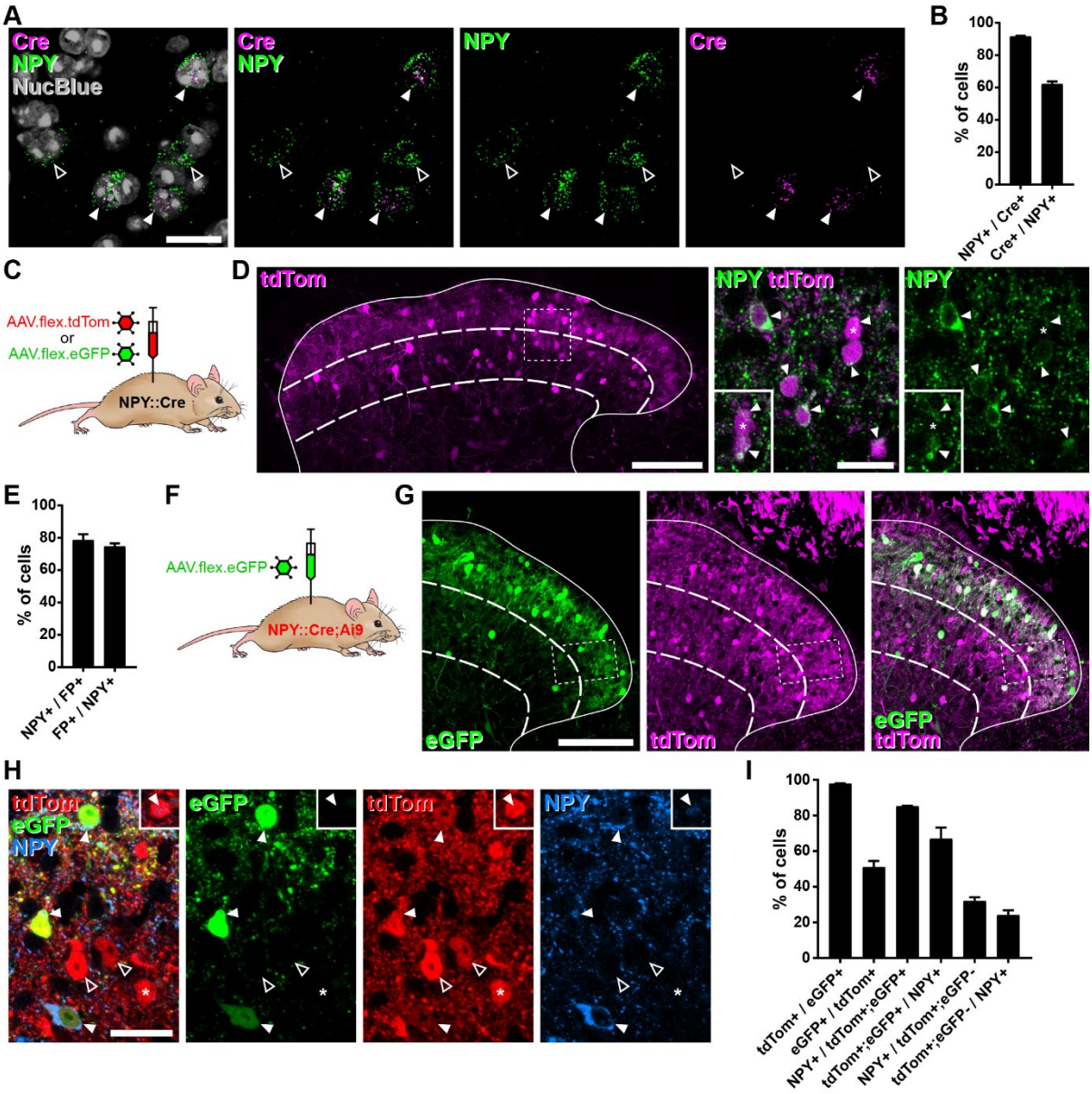

1378

1379 **Figure 1. Cre-dependent AAV injections in young adult NPY::Cre mice target**
1380 **dorsal horn inhibitory NPY interneurons and avoid transient NPY-expressing**
1381 **cells.** (**A**) In situ hybridisation for *Cre* (magenta) and *Npy* (green) mRNA in the mid-
1382 lumbar dorsal horn. Sections were counterstained with NucBlue (grey) to reveal
1383 nuclei. Three *Cre*-positive cells are also positive for *Npy* (filled arrowheads), and
1384 there are two cells that are positive for *Npy* only (open arrowheads). Scale bar =
1385 20µm. (**B**) Quantification of co-expression of *Cre* and *Npy* mRNA in laminae I-III (n =
1386 3 mice). (**C**) The experimental approach used to generate the data presented in **D**
1387 and **E**. (**D**) Co-expression of tdTomato (tdTom; magenta) and NPY (green)

Click here to enter text.

immunoreactivity in mid-lumbar dorsal horn of an NPY::Cre mouse injected with AAV.flex.tdTom in adulthood. Low power image shows tdTomato-positive cells throughout laminae I-III (scale bar = 100 μm). High power images (corresponding to the box in the low power image) demonstrate the high degree of co-localisation of tdTomato expression and NPY immunoreactivity (filled arrowheads; scale bar = 20μm). Insets show clearer NPY labelling in a different z-plane for the cell marked with an asterisk and the cell immediately below it. (**E**) Quantification of co-expression of fluorescent protein (FP) and NPY in laminae I-III of NPY::Cre mice injected with AAV.flex.tdTom or AAV.flex.eGFP at adulthood (n = 3 mice; 2 injected with AAV.flex.tdTomato and 1 with AAV.flex.eGFP). (**F**) The experimental approach taken for the data presented in **G-I**. (**G**) Expression of tdTomato and eGFP in mid-lumbar dorsal horn of an NPY::Cre;Ai9 mouse injected with AAV.flex.eGFP in adulthood. eGFP-positive cells (green) are a subset of a broader population of tdTomato-positive cells (magenta; scale bar = 100 μm). (**H**) High power images corresponding to boxed area in **G** showing three tdTom+/eGFP+ (red and green, respectively) double-labelled cells (filled arrowheads) that are also NPY immunoreactive (blue). Open arrowheads mark two cells positive for tdTomato only. The asterisk marks a tdTomato-positive/eGFP-negative cell that is also NPY immunoreactive, though this is only apparent in a different z-plane (insets). Scale bar = 20μm. (**I**) Quantification of co-expression of tdTomato, eGFP and NPY in laminae I-III of NPY::Cre;Ai9 mice injected with AAV.flex.eGFP at adulthood (n = 2 mice). Solid lines in low power images in **D** and **G** denote the grey/white matter border, curved dashed lines denote the boundaries of lamina III and dashed boxes denote the regions shown in corresponding high power images. Data are shown as mean ± SEM.

Click here to enter text.

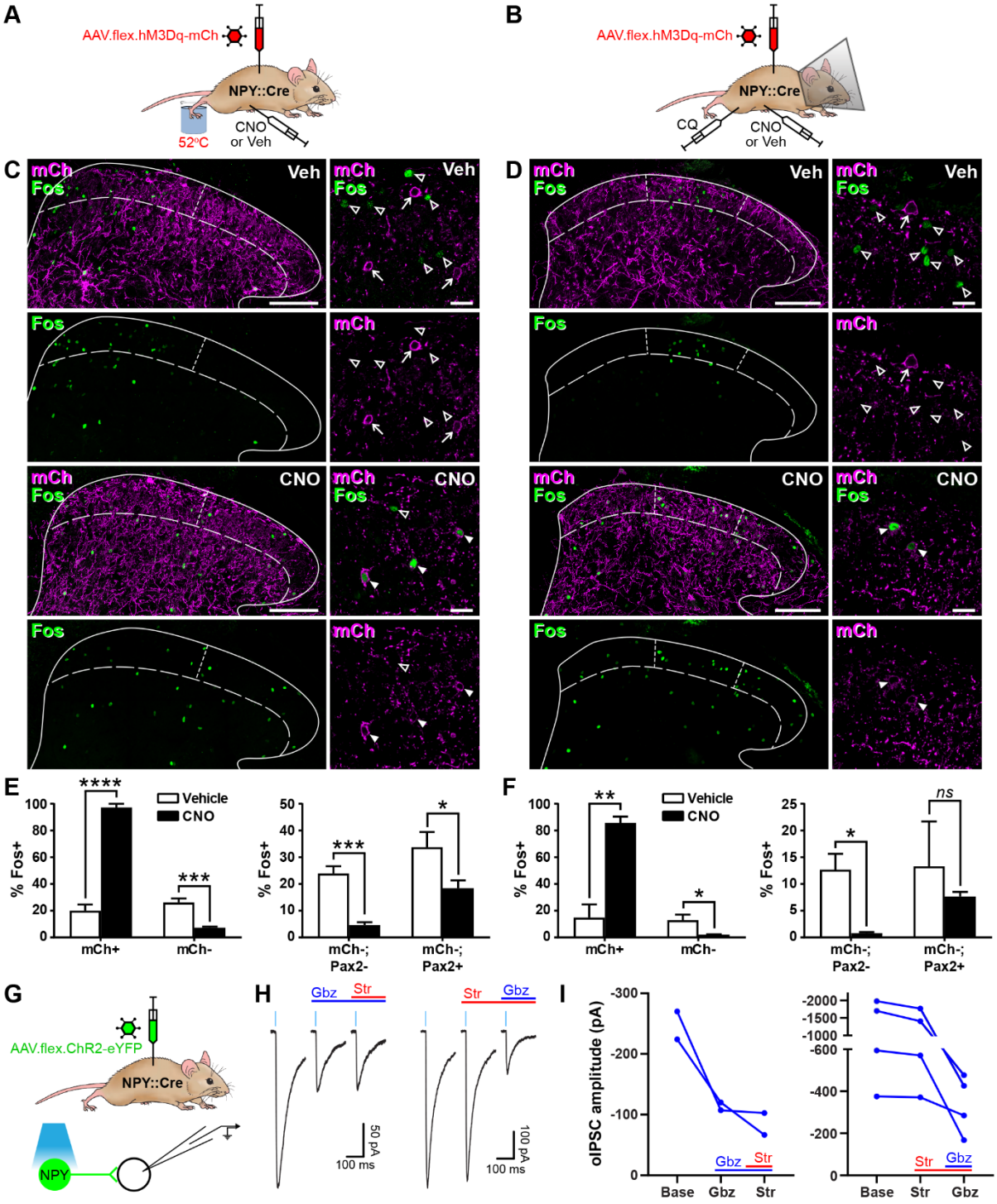

Figure 2. Activation of inhibitory NPY interneurons reduces activity in dorsal horn circuits recruited by noxious and pruritic stimuli. (**A, B**) The experimental approaches used to generate the data presented in **C**,**E**, and **D**,**F**, respectively. (**C**, **D**) Low power images show mCherry expression (mCh; magenta) and Fos immunoreactivity (green) in L4 (**C**) or L3 (**D**) dorsal horn of NPY::Cre mice that had been injected with AAV.flex.hM3Dq-mCherry and treated with vehicle control (Veh) or CNO 30 minutes prior to a noxious heat stimulus (immersion of the hindpaw in

Click here to enter text.

1420 52ºC water; **C**) or a pruritic stimulus (intradermal injection of 100 µg chloroquine, CQ,
1421 dissolved in 10 µl PBS into the calf; **D**) and perfusion-fixed 2 hours post-stimulation.
1422 In vehicle-treated animals, Fos expression is observed in the somatotopically-
1423 relevant area of the superficial laminae (left of short dashed line in **C**; between short
1424 dashed lines in **D**). In CNO-treated animals, Fos expression is observed in hM3Dq-
1425 mCherry-expressing cells, but is reduced in surrounding hM3Dq-mCherry-negative
1426 cells within the somatotopically-relevant area. This is demonstrated in the high
1427 magnification images (to the right of the main image in each case), where filled
1428 arrowheads mark examples of hM3Dq-mCherry-expressing cells immunoreactive for
1429 Fos, open arrowheads mark Fos-positive cells that lack hM3Dq-mCherry and arrows
1430 mark hM3Dq-mCherry-expressing cells that are negative for Fos. Scale bars; 100
1431 µm (low power images), 20 µm (high power images). Solid lines in **C** and **D** denote
1432 the grey/white matter border, curved dashed lines denote the lamina II/III border. (**E**,
1433 **F**) Left-hand graphs show quantification of the proportion of hM3Dq-mCherry-
1434 positive (mCh+) and -negative (mCh-) cells that display Fos immunoreactivity in
1435 vehicle- or CNO-treated mice that received a noxious heat (**E**; n = 3 mice for vehicle,
1436 4 for CNO) or pruritic (**F**; n = 6 for both groups) stimulus. Right-hand graphs in **E** and
1437 **F** show quantification of the proportion of hM3Dq-mCherry-negative cells that display
1438 Fos immunoreactivity, separated into excitatory (Pax2-) and inhibitory (Pax2+)
1439 populations. Analyses were performed within the somatotopically-relevant areas of
1440 laminae I and II. (**G**) The experimental approach used to generate the data
1441 presented in **H** and **I**. (**H**) Representative oIPSCs recorded in unlabelled (ChR2-
1442 eYFP-negative) cells in spinal cord slices from NPY::Cre mice that had received
1443 intraspinal injections of AAV.flex.ChR2-YFP. Recordings were made in the absence
1444 and presence of gabazine (Gbz) and strychnine (Str). Traces show an average of 6
1445 stimuli, light blue bars denote period of optogenetic stimulation. Note that in the
1446 presence of high intracellular Cl- concentration, IPSCs appear as inward currents. (**I**)
1447 Quantification of the mean peak amplitude of oIPSCs recorded in the absence
1448 (Base) and presence of gabazine and strychnine. Data are shown as mean ± SEM.
1449 *$p < 0.05$, ***$p < 0.001$; unpaired t-test with Holm-Šidák correction for multiple
1450 comparisons. Data are shown as mean ± SEM in (**E** and **F**) and individual values in
1451 (**I**).

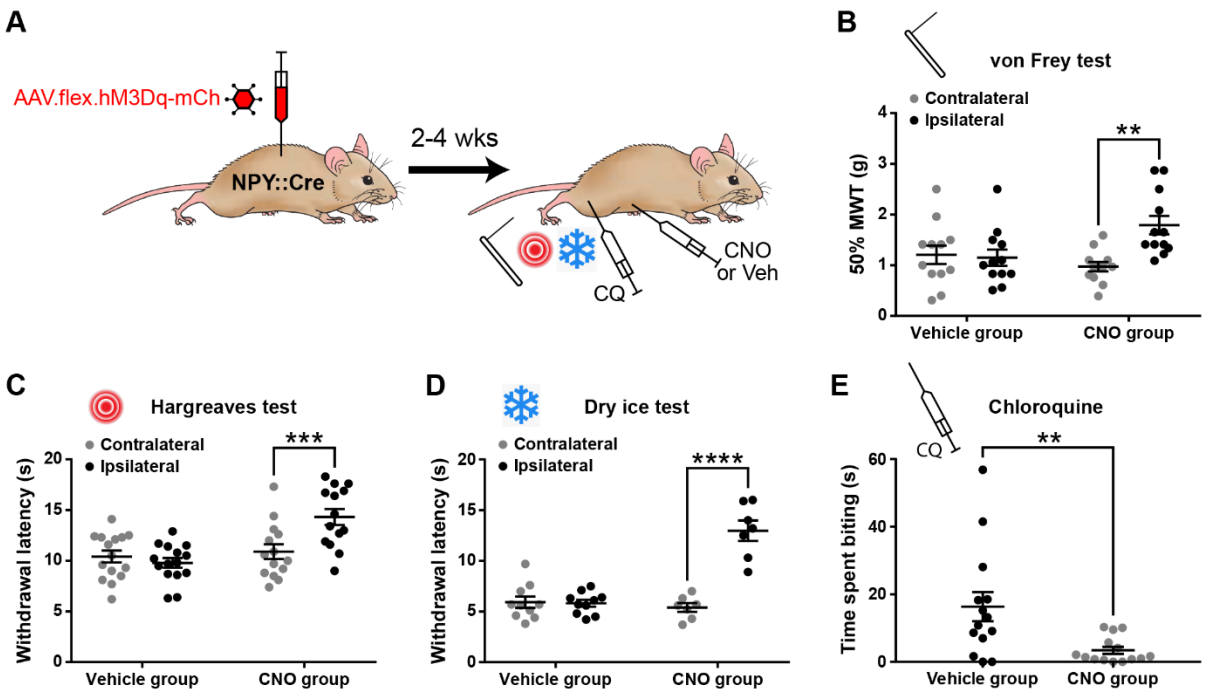

Figure 3. Activation of inhibitory NPY interneurons increases acute nociceptive thresholds and reduces pruritogen-evoked itch behaviour. (**A**) The experimental approach used to generate the data presented in **B-E**. (**B-D**) AAV.flex.hM3Dq-mCherry spinal-injected NPY::Cre mice display an increased mechanical withdrawal threshold (MWT) (**B**; n = 12 vehicle group, 12 CNO group) and increased withdrawal latencies to radiant heat (**C**; n = 15 vehicle group, 14 CNO group) and to cold (**D**; n = 10 vehicle group, 7 CNO group) of the ipsilateral hindpaw following CNO injection, but not vehicle control injection. (**E**) AAV.flex.hM3Dq-mCherry spinal-injected mice spend significantly less time biting the calf region in the 30 minutes following intradermal injection of chloroquine when injected with CNO, compared to vehicle-treated controls (n = 14 vehicle group, 14 CNO group). Data are shown as individual values with mean ± SEM. **$p < 0.01$, ***$p < 0.001$, ****$p < 0.0001$; repeated-measures 2-way ANOVA with Šidák's post-test in (**B-D**); unpaired t-test in (**E**).

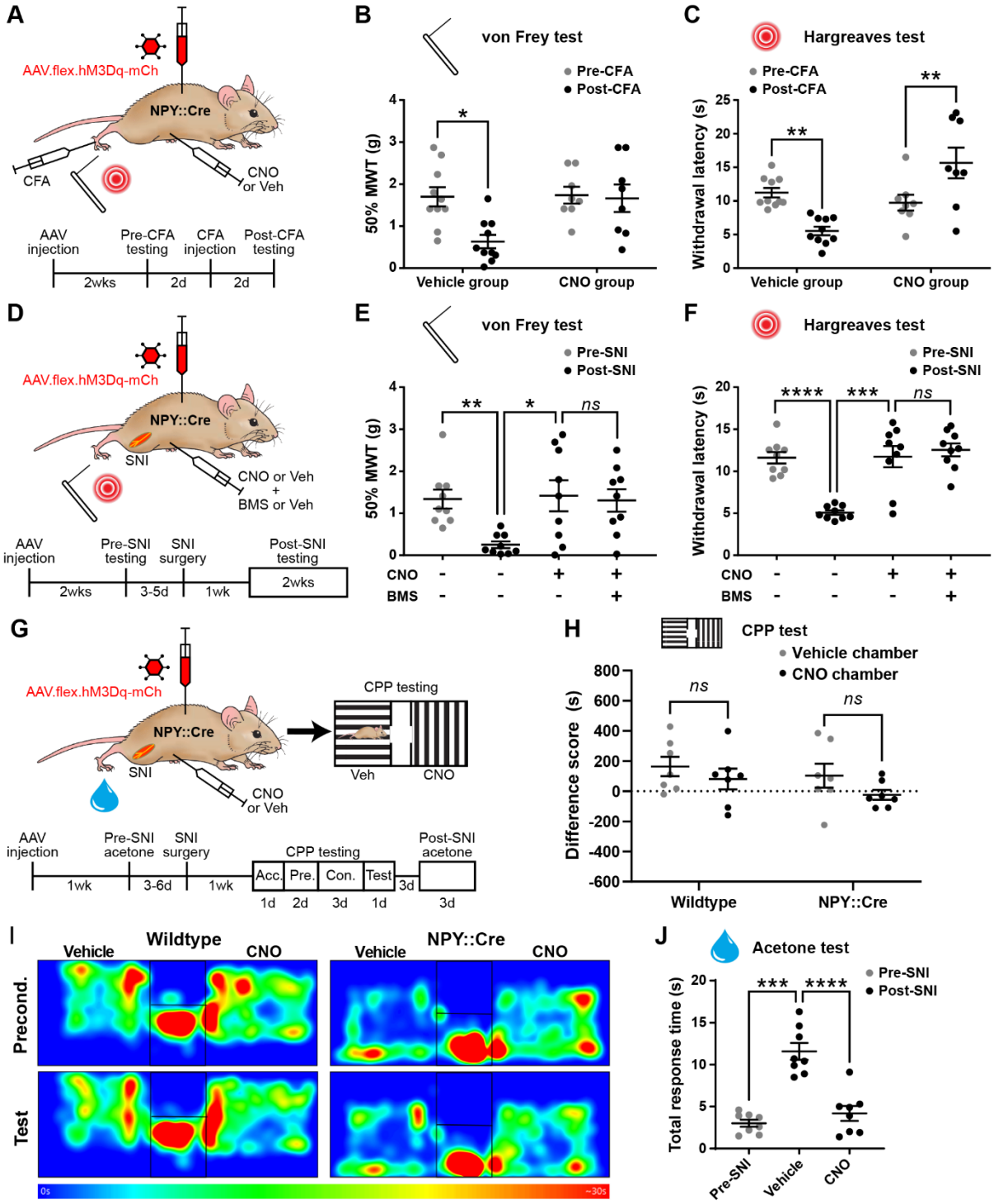

Figure 4. Activation of inhibitory NPY interneurons blocks mechanical and thermal hypersensitivity in models of inflammatory and neuropathic pain. (**A**) The experimental approach taken to generate the data presented in **B** and **C**. (**B**, **C**) Vehicle control-treated AAV.flex.hM3Dq-mCherry spinal-injected NPY::Cre mice display marked reductions in mechanical withdrawal threshold (MWT) (**B**) and withdrawal latency to radiant heat (**C**) of the ipsilateral paw 2 days after intraplantar injection of complete Freund's adjuvant (CFA). Both mechanical and thermal

Click here to enter text.

hypersensitivity are blocked in CNO-treated mice (n = 10 vehicle group, 8 CNO group). (**D**) The experimental approach taken for the data presented in **E** and **F**. Drug treatments were administered using a crossover design (n = 9). (**E**, **F**) Marked reductions in mechanical withdrawal threshold (MWT) (**E**) and withdrawal latency to radiant heat (**F**) are observed following spared nerve injury (SNI). These are blocked by CNO treatment, and this blockade persists in the presence of the Y1 antagonist BMS 193885 (BMS). (**G**) The experimental approach taken for the data presented in **H - J**. Acc. = acclimation; Pre. = pre-conditioning; Con. = conditioning. (**H**) Neither wildtype control nor AAV.flex.hM3Dq-mCherry spinal-injected NPY::Cre mice displayed a conditioned place preference (CPP) to CNO following SNI (n = 7). (**I**) Heat maps of a representative mouse from each group demonstrating position and time spent in each chamber during preconditioning and post-conditioning test days. (**J**) A marked increase in the time spent responding to application of acetone to the ipsilateral paw (shaking, lifting and/or licking) is seen in vehicle-treated AAV.flex.hM3Dq-mCherry spinal-injected NPY::Cre mice following SNI. This cold hypersensitivity is blocked when the same mice are treated with CNO. Data are shown as individual values with mean ± SEM. *$p < 0.05$, **$p < 0.01$, ***$p<0.001$, ****$p < 0.0001$; repeated-measures 2-way ANOVA with Šidák's post-test in (**B**, **C, H**), repeated-measures 1-way ANOVA with Šidák's post-test in (**E**, **F & J)**.

Click here to enter text.

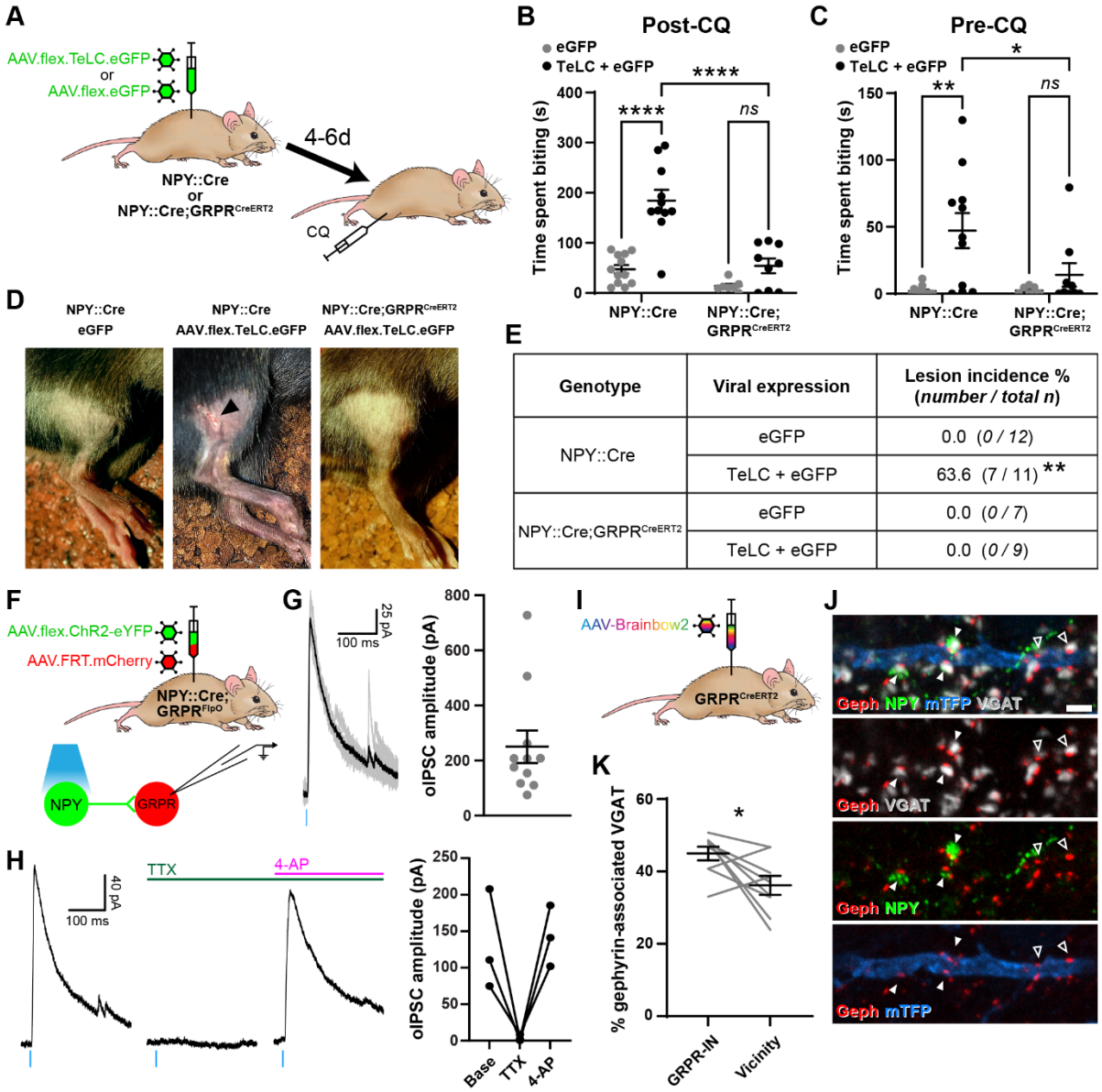

Genotype	Viral expression	Lesion incidence % (*number / total n*)
NPY::Cre	eGFP	0.0 (*0 / 12*)
	TeLC + eGFP	63.6 (7 / 11) **
NPY::Cre;GRPR^{CreERT2}	eGFP	0.0 (*0 / 7*)
	TeLC + eGFP	0.0 (*0 / 9*)

Figure 5. Increased itch caused by silencing NPY interneurons operates through a circuit involving GRPR-expressing excitatory interneurons. (**A**) The experimental approach used to generate the data presented in **B-E**. (**B**) Silencing of NPY-INs by viral expression of tetanus toxin light chain (TeLC) in AAV.flex.TeLC.eGFP spinal-injected NPY::Cre mice results in a significant enhancement of chloroquine-evoked itch (Post-CQ), compared to that seen in AAV.flex.eGFP-injected controls. This enhancement of CQ-evoked itch is significantly reduced when NPY- and GRPR-INs are simultaneously silenced by injecting AAV.flex.TeLC.eGFP into NPY::Cre;GRPR^{CreERT2} mice. The numbers of mice per group are as outlined in the table in **E**. (**C**) Silencing of NPY-INs by TeLC also results in the development of spontaneous itch behaviour as assessed over 30 minutes prior to CQ administration (Pre-CQ). This spontaneous itch is also

Click here to enter text.

1507 significantly reduced when GRPR-INs are simultaneously silenced. (**D**)
1508 Representative images of a skin lesion on the calf of an AAV.flex.TeLC.eGFP-
1509 injected NPY::Cre mouse (arrowhead, middle image), and the lack of lesions in
1510 AAV.flex.eGFP-injected NPY::Cre or AAV.flex.TeLC.eGFP-injected
1511 NPY::Cre;GRPR^{CreERT2} mice. (**E**) Table outlining the incidence of lesions in
1512 AAV.flex.eGFP- or AAV.flex.TeLC.eGFP-injected NPY::Cre or NPY::Cre;
1513 GRPR^{CreERT2} mice. Lesions were observed in approximately two-thirds of
1514 AAV.flex.TeLC.eGFP-injected NPY::Cre mice, but never in AAV.flex.TeLC.eGFP-
1515 injected NPY::Cre; GRPR^{CreERT2} mice, nor in AAV.flex.eGFP-injected control groups.
1516 (**F**) The experimental approach used to generate the data presented in **G** and **H**. (**G**)
1517 Optogenetic activation of NPY-INs induces monosynaptic oIPSCs in GRPR-INs.
1518 Representative traces of oIPSCs recorded in a GRPR neuron are shown on the left,
1519 with 6 individual oIPSCs in grey and an averaged trace in black. Quantification of the
1520 mean peak amplitude of oIPSCs recorded in 11 GRPR-INs is shown on the right. For
1521 all 11 cases, all 6 light stimuli resulted in oIPSCs with no failures. (**H**) Example traces
1522 from a GRPR-IN (left) show that oIPSCs are blocked by TTX and reinstated by 4-AP;
1523 quantification of mean peak oISPC amplitude from 3 GRPR-INs is shown on the
1524 right. (**I**) The experimental approach used to generate the data presented in **J** and **K**.
1525 (**J**) Filled arrowheads mark three examples of NPY-immunoreactive (green)
1526 inhibitory boutons synapsing onto dendrite of a Brainbow-labelled GRPR-IN (mTFP,
1527 blue). Inhibitory synapses were defined as VGAT-positive profiles (grey) in contact
1528 with gephyrin puncta (red). Open arrowheads mark two examples of NPY-negative
1529 inhibitory synapses on the Brainbow-labelled dendrite. Scale bar = 2μm. (**K**)
1530 Quantification of the percentage of inhibitory synapses on to 9 GRPR-INs, or in the
1531 vicinity of those cells, at which the presynaptic VGAT bouton is NPY-
1532 immunoreactive. Data are shown as individual values with mean ± SEM in (**B**, **C** and
1533 **G**), individual values in (**H**) and individual matched values with mean ± SEM in (**K**).
1534 *$p < 0.05$, **$p < 0.01$, ****$p < 0.0001$; 2-way ANOVA with Tukey's post-test in (**B** and
1535 **C**), Fisher's exact test with Bonferroni correction in (**E**) and Wilcoxon matched pairs
1536 test in (**K**).

1537

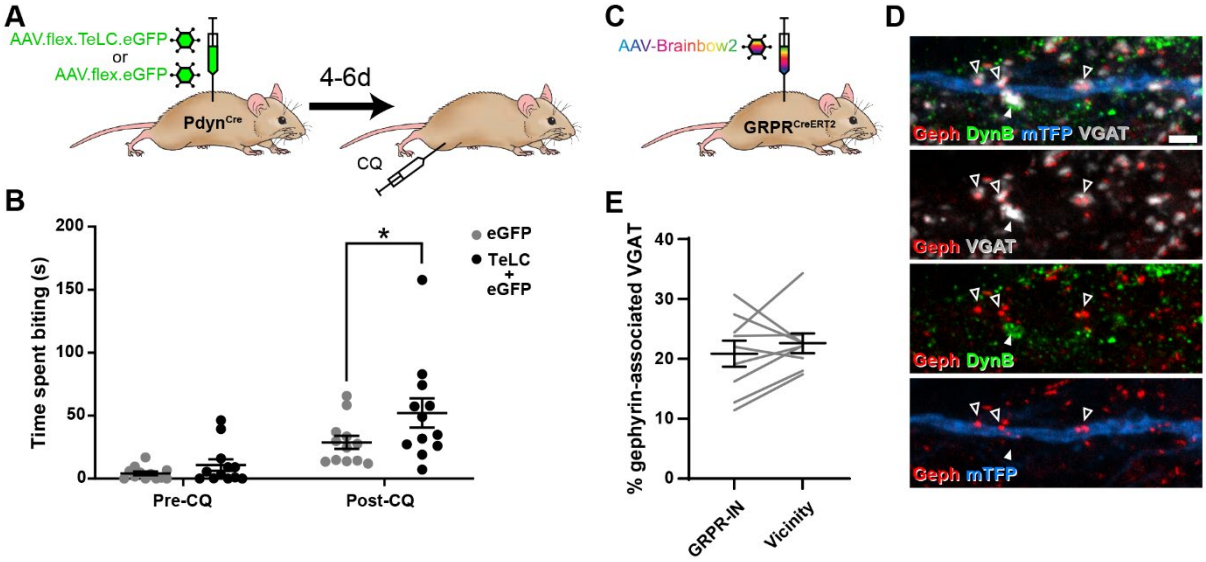

1538

1539 **Figure 6. Toxin-mediated silencing of Dynorphin-expressing inhibitory**
1540 **interneurons enhances pruritogen-evoked itch.**
1541 (**A**) The experimental approach used to generate the data presented in **B**. (**B**)
1542 Silencing of Dyn-INs by viral expression of tetanus toxin light chain (TeLC) in Pdyn^{Cre}
1543 mice results in a significant enhancement of chloroquine-evoked itch (Post-CQ),
1544 compared to eGFP-expressing controls ($p = 0.0379$; repeated-measures 2-way
1545 ANOVA with Šidák's post-test). No significant difference was observed in biting time
1546 prior to injection with chloroquine (Pre-CQ; $p = 0.7431$; n= 12 for both GFP and
1547 TeLC groups). (**C**) The experimental approach used to generate the data presented
1548 in **D** and **E**. (**D**) Filled arrowhead marks an example of a DynB-expressing (green)
1549 inhibitory bouton synapsing onto dendrite of a Brainbow-labelled GRPR-IN (mTFP,
1550 blue). Inhibitory synapses were defined as VGAT-positive profiles (grey) in contact
1551 with gephyrin puncta (red). Open arrowheads mark three examples of DynB-
1552 negative inhibitory synapses on the Brainbow-labelled dendrite. Scale bar = 2μm. (**E**)
1553 Quantification of the percentage of total inhibitory synapses on to 9 GRPR-INs, or in
1554 the vicinity of those cells, that contain DynB. No significant difference was observed
1555 between these proportions ($p=0.3438$; Wilcoxon matched pairs test). Data are shown
1556 as individual values with mean ± SEM in (**B**) and individual matched values with
1557 mean ± SEM in (**E**).

Click here to enter text.

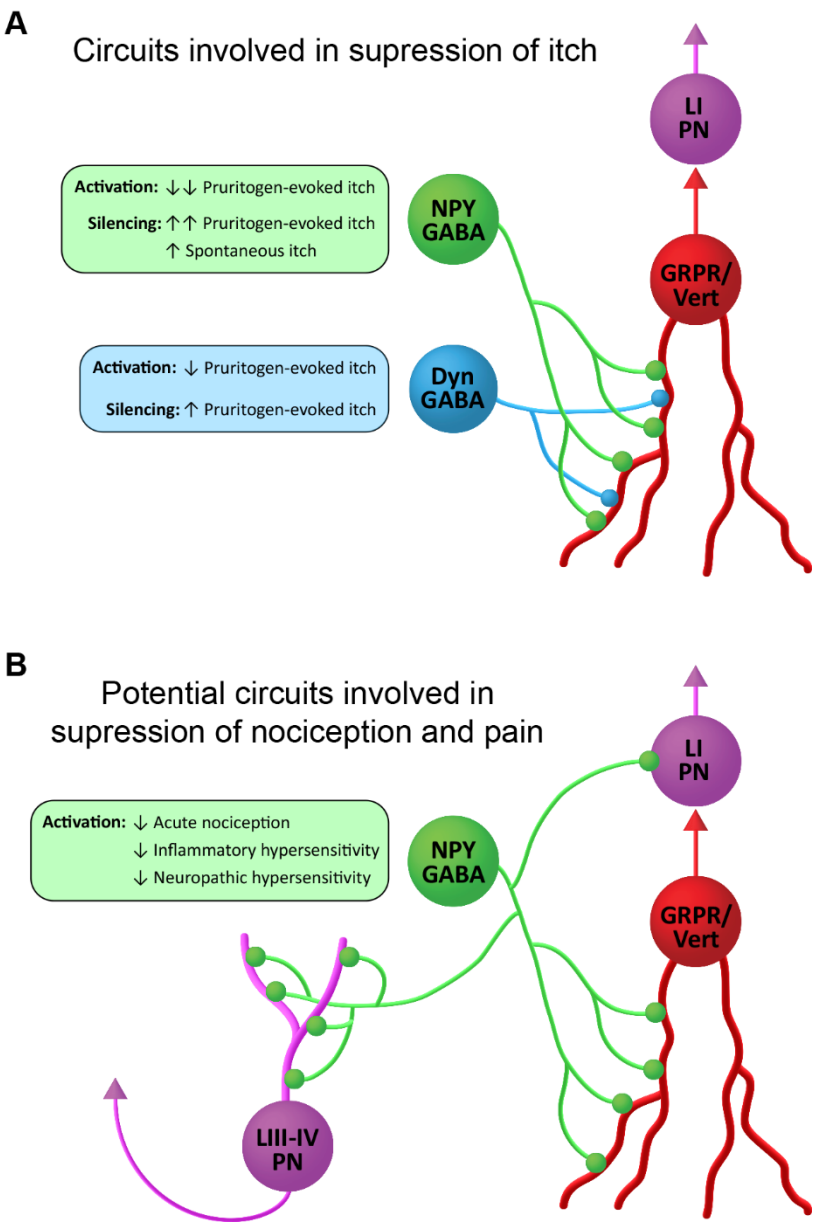

Figure 7. Suggested roles of NPY-expressing inhibitory interneurons in spinal itch and pain circuits. (**A**) Circuits involved in suppression of itch. NPY-INs provide a high proportion (45%) of the inhibitory synapses on GRPR-expressing excitatory interneurons. The GRPR cells have vertical (Vert) morphology and are thought to transmit itch- and pain-related information to spinal projection neurons in lamina I (LI PNs). Pruritogen-evoked itch is markedly reduced by NPY-IN activation, while silencing of NPY-INs enhances pruritogen-evoked itch and results in spontaneous itch. Dyn-INs also provide inhibitory input to GRPR cells, but only account for ~20% of their inhibitory synapses. Silencing of Dyn-INs increases pruritogen-evoked itch, but to a lesser degree than NPY-IN silencing, and without the appearance of

spontaneous itch. Activation of Dyn-INs has previously been shown to reduce itch in response to a range of pruritogens (see Huang et al. 2018). (**B**) Potential circuits involved in suppression of nociception and pain. Vertical cells are thought to be involved in the transmission of both normal and pathological pain signals through their input to LI PNs. Chemogenetic activation of GRPR-expressing vertical cells elicits both itch- and pain-related behaviours (Polgár et al 2022). NPY-INs may therefore act to supress acute nociception, as well as inflammatory and neuropathic hypersensitivity, via inhibition of vertical cells. Additionally, NPY-INs have previously been shown to directly innervate nociceptive projection neurons of the anterolateral system in lamina I and laminae III-IV (LIII-IV PN).

1580 **FIGURE SUPPLEMENTS**

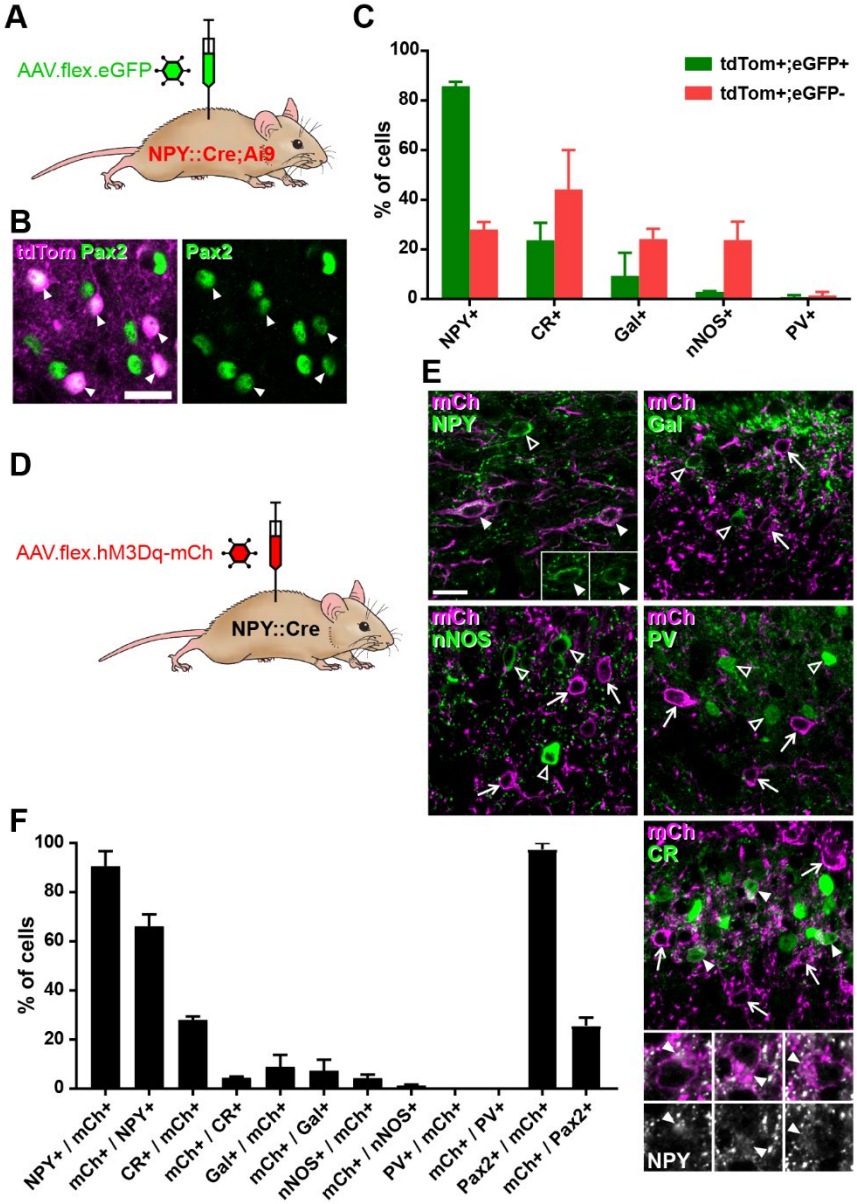

1581

1582 **Figure 1 – figure supplement 1. Cre-dependent AAV injections in young adult**
1583 **NPY::Cre mice target dorsal horn inhibitory NPY interneurons and avoid**
1584 **transient NPY-expressing cells.** (**A**) The experimental approach used to generate
1585 the data shown in **B** and **C**. (**B**) Co-expression of tdTomato (tdTom; magenta) and
1586 Pax2 (green) in the mid-lumbar dorsal horn of an adult NPY::Cre;Ai9 mouse. All
1587 tdTomato-positive cells are also Pax2 immunoreactive (filled arrowheads; scale bar =
1588 20 μm). (**C**) Quantification of the proportion of tdTom+/eGFP+ double-labelled cells
1589 and tdTomato-positive, eGFP-negative cells (tdTom+/eGFP-) that express various
1590 inhibitory interneuron neurochemical markers in laminae I and II of NPY::Cre;Ai9
1591 mice that were injected with AAV.flex.eGFP in adulthood (n = 2 mice). (**D**) The

experimental approach used to generate the data shown in **E** and **F**. (**E**) Micrographs demonstrating the distribution of hM3Dq-mCherry expression (mCh, magenta) and immunoreactivity for various inhibitory interneuron neurochemical markers (green) in mid-lumbar dorsal horn of an NPY::Cre mouse injected with AAV.flex.hM3Dq-mCherry in adulthood (Gal, galanin; nNOS, neuronal nitric oxide synthase; PV, parvalbumin; CR, calretinin). Arrows mark cells labelled with mCherry only, open arrowheads mark cells positive for the neurochemical marker only and filled arrowheads mark cells that express both hM3Dq-mCherry and the neurochemical marker. Insets in the NPY image show NPY staining only for the cells marked with filled arrowheads to demonstrate the NPY immunoreactivity in these cells. Higher magnification images below the CR image show NPY immunoreactivity (grey) in the cells marked with filled arrowheads. Scale bar = 20μm. (**F**) Quantification of co-expression of hM3Dq-mCherry and the various inhibitory interneuron neurochemical markers in laminae I and II of NPY::Cre mice injected with AAV.flex.hM3Dq-mCherry in adulthood (n = 3 mice). Data are shown as mean ± SEM.

Click here to enter text.

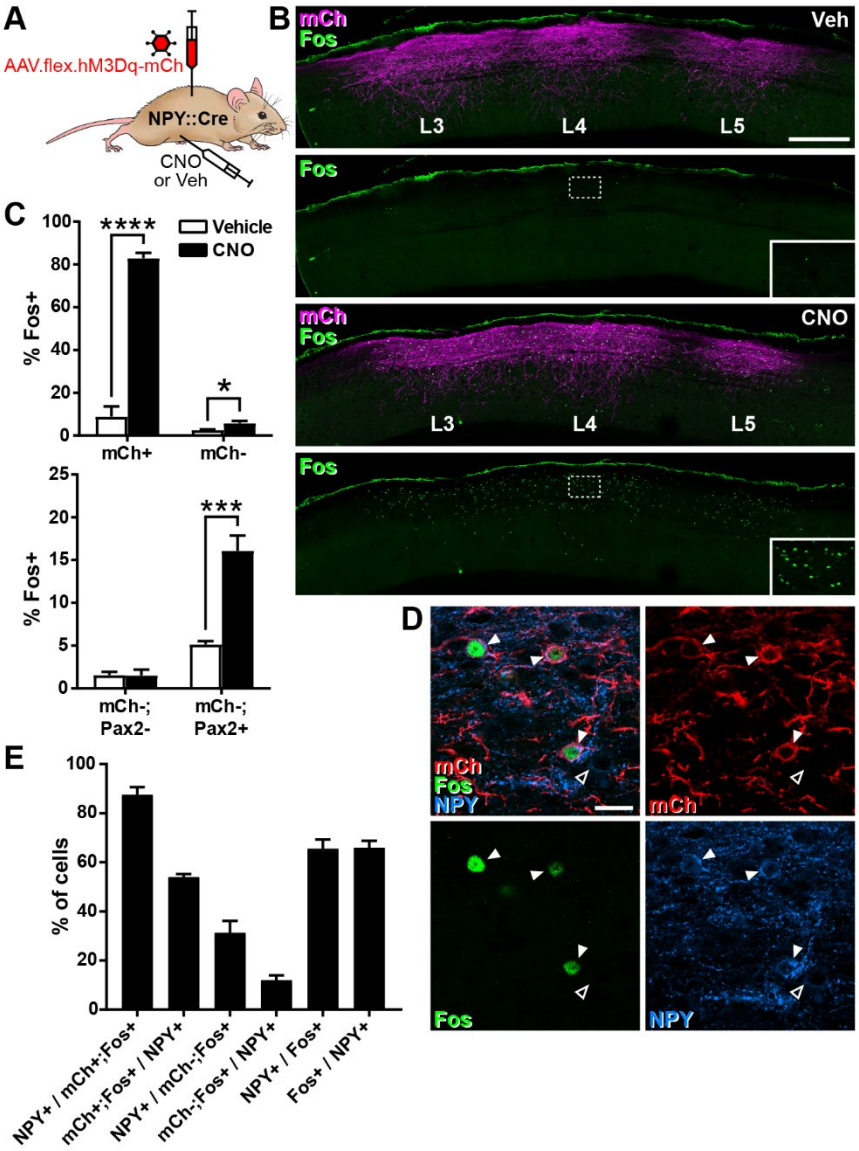

Figure 2 – figure supplement 1. CNO-mediated activation of dorsal horn inhibitory NPY interneurons in NPY::Cre mice injected with AAV.flex.hM3Dq-mCherry. (**A**) The experimental approach used to generate the data shown in this figure. (**B**) Sagittal sections through the ipsilateral side of the L3-5 spinal cord segments of NPY::Cre mice injected with AAV.flex.hM3Dq-mCherry at L3, L4 and L5 levels and treated with vehicle control (Veh) or CNO two hours prior to perfusion fixation. hM3Dq-mCherry expression (mCh, magenta) can be seen extending through the L3-5 dorsal horn in both animals. Fos-positive cells (green) are infrequent in the vehicle-treated animal, but are numerous in the CNO-treated mouse and correspond to the area of hM3Dq-mCh expression. Dashed boxes indicate the areas shown at higher magnification in the insets. Scale bar = 500 μm. (**C**) Top graph shows quantification of the proportion of hM3Dq-mCherry-positive (mCh+) and

-negative (mCh-) cells in laminae I-III that display Fos immunoreactivity in vehicle- or CNO-treated mice. Bottom graph shows quantification of the proportion of hM3Dq-mCherry-negative cells in laminae I-III that display Fos immunoreactivity in vehicle- or CNO-treated mice, separated into excitatory (Pax2-) and inhibitory (Pax2+) populations. *$p < 0.05$, ***$p < 0.001$, ****$p < 0.0001$; unpaired t-test with Holm-Šidák correction for multiple comparisons.; n = 4. (**D**) Example confocal image demonstrating co-expression of hM3Dq-mCh (red), Fos (green) and NPY (blue) in L4 dorsal horn of an NPY::Cre mouse that had been injected with AAV.flex.hM3Dq-mCherry and treated with CNO 2 hours prior to perfusion fixation. Three hM3Dq-mCherry-positive cells that are immunoreactive for both Fos and NPY are highlighted (filled arrowheads). A weakly NPY-positive cell that lacks both hM3Dq-mCherry and Fos expression can also be seen (open arrowhead). Scale bar = 20 µm. (**E**) Quantification of co-expression of hM3Dq-mCherry, Fos and NPY in laminae I-III in the L4 segment of mice treated with CNO two hours prior to perfusion fixation (n = 4). Data are shown as mean ± SEM.

Click here to enter text.

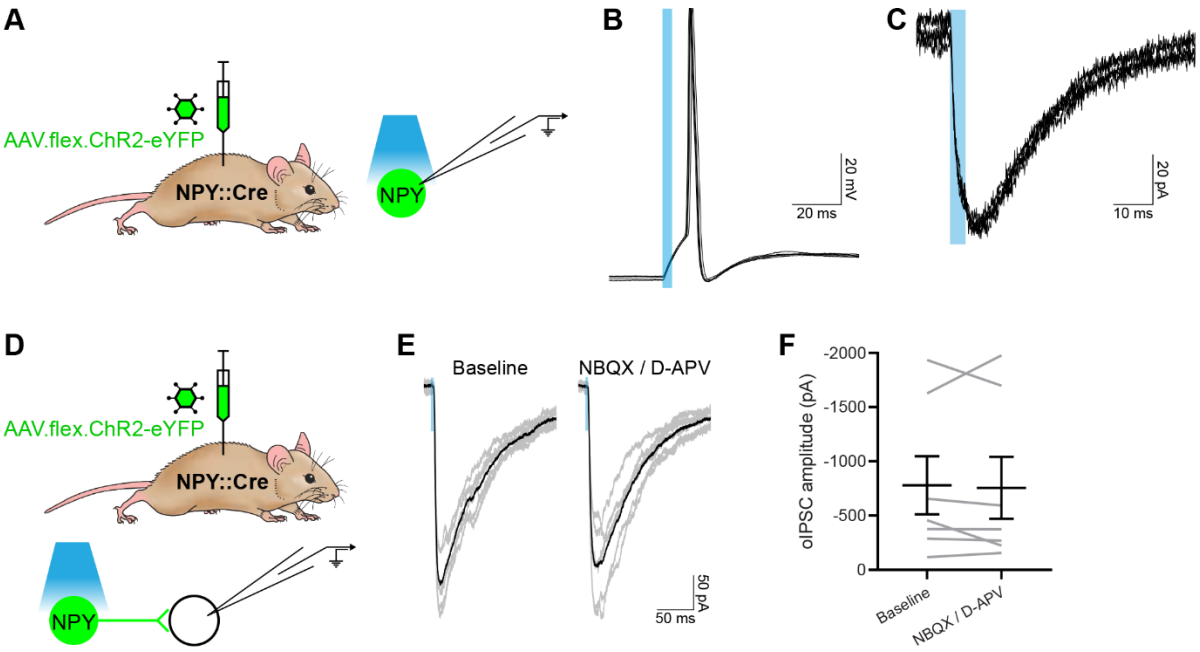

Figure 2 – figure supplement 2. Characterisation of optogenetic activation of NPY-INs. (**A**) The experimental approach used to generate data presented in **B** and **C**. (**B**, **C**) Representative traces showing optogenetically evoked action potential firing (**B**) and currents (**C**) in an NPY-IN labelled with ChR2-eYFP. Each trace displays 6 stimuli. (**D**) The experimental approach used to generate data presented in **E** and **F**. (**E**) Representative traces of oIPSCs recorded in unlabelled (ChR2-eYFP-negative) cells in the absence (Baseline) and presence of NBQX and D-APV, 6 individual oIPSCs are shown in grey and an averaged trace in black. (**F**) Quantification of the mean peak amplitude of oIPSCs recorded in the absence and presence of NBQX and D-APV. Blue boxes in **B**, **C** and **E** denote the period of optogenetic stimulation. Data are shown as individual matched values with mean ± SEM.

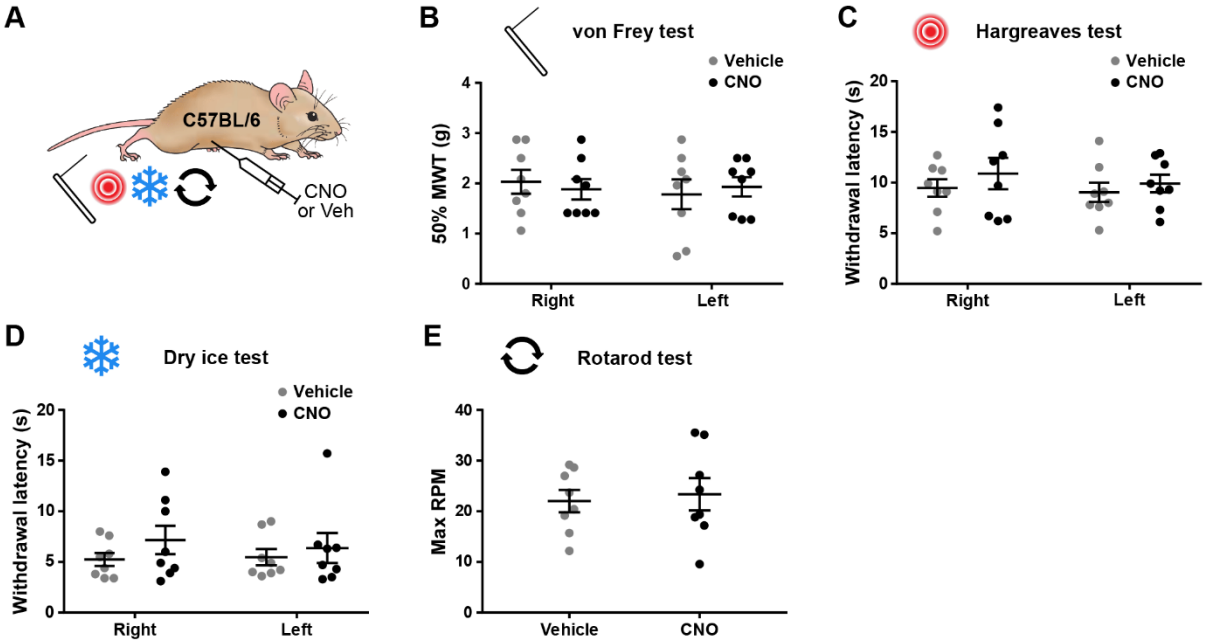

Figure 3 – figure supplement 1. Injection of 5 mg/kg clozapine-N-oxide does not result in off-target behavioural effects. (**A**) The experimental approach used to generate data presented in this figure. Eight naïve wildtype C57BL/6 mice were injected with 5 mg/kg CNO or vehicle control using a cross-over experimental design and tested for mechanical withdrawal thresholds (MWT; **B**), as well as withdrawal latencies to heat (**C**) and cold (**D**) on both hindpaws. General motor co-ordination was assessed using the accelerating rotarod test (**E**). No significant differences were seen between treatments for either paw in any of the nociceptive tests (repeated-measures 2-way ANOVA with Šidák's post-test), or in the maximum RPM in the accelerating rotarod test (paired t test). Data are shown as individual values with mean ± SEM.

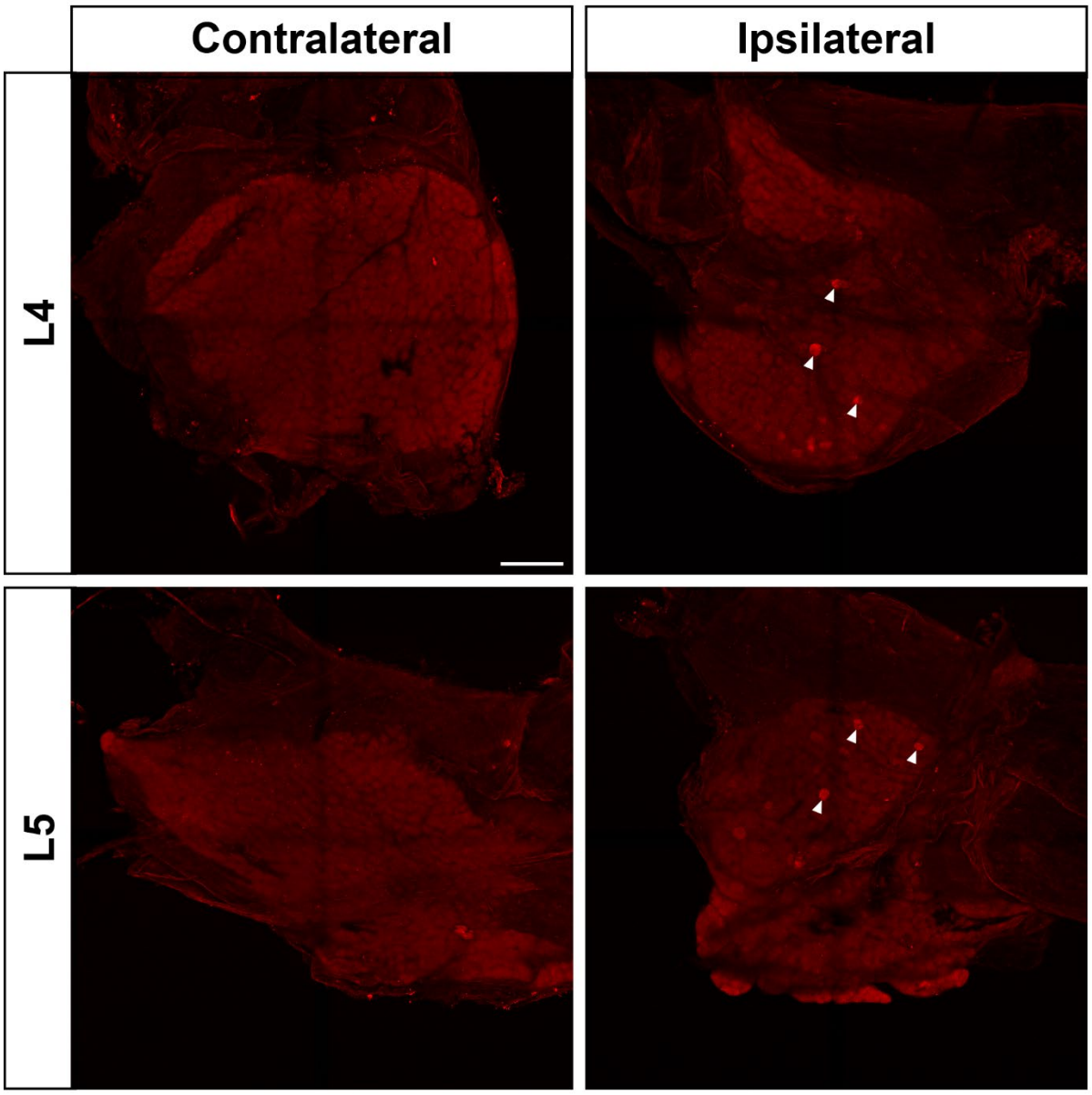

	Contralateral	Ipsilateral
L4	0.0 ± 0.0 (*0 – 0*)	12.5 ± 2.3 (*9 -19*)
L5	0.0 ± 0.0 (*0 – 0*)	17.5 ± 3.6 (*9 -26*)

Figure 4 – figure supplement 1. Spared nerve injury results in minimal ipsilateral hM3Dq expression in L4/5 DRG of AAV.flex.hM3Dq-mCherry spinal-injected NPY::Cre mice. Maximum-intensity projections of confocal image stacks from contralateral and ipsilateral (with regards to AAV injection and spared nerve injury) L4 and L5 whole-mount dorsal root ganglia (DRG) from an AAV.flex.hM3Dq-mCherry spinal-injected NPY::Cre mouse perfused 4 weeks following SNI surgery. As expected, no hM3Dq-mCherry-positive cells were detected in the contralateral

1668 DRGs. On the ipsilateral side, a small number of hM3Dq-mCherry-positive cells were
1669 observed in both L4 and L5 DRGs (filled arrowheads mark examples). Scale bar =
1670 200 μm. The table shows quantification of mCherry-labelled cells on the contralateral
1671 and ipsilateral sides (n = 4; values are mean ± SEM (*range*)).

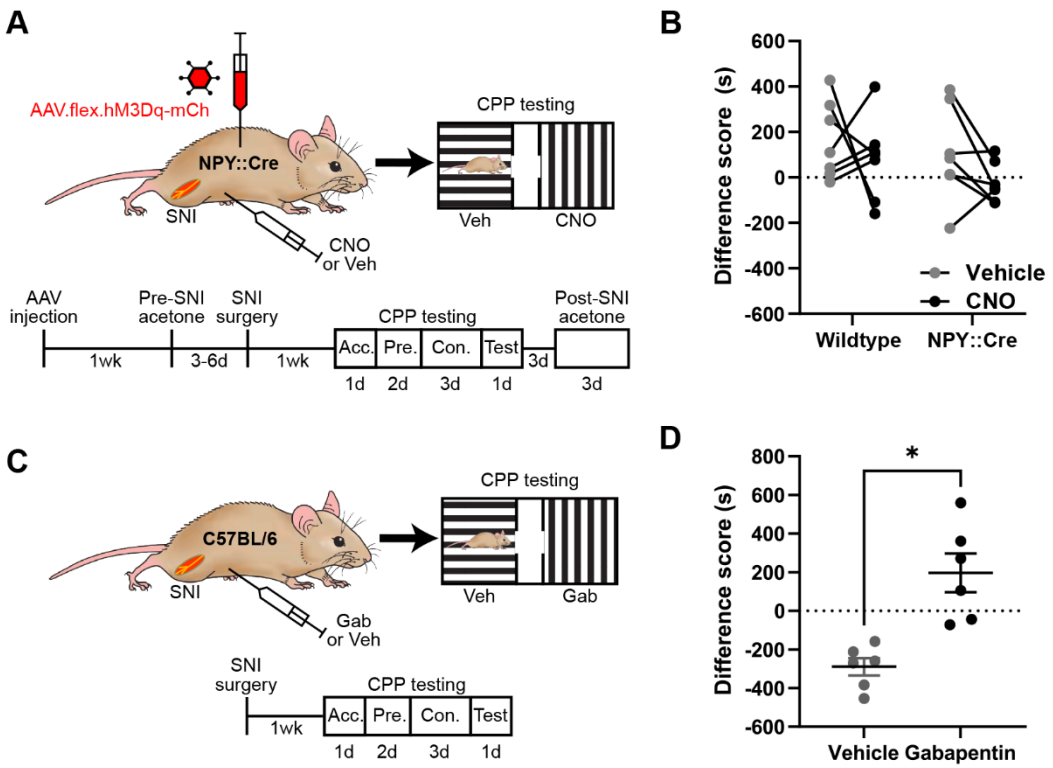

Figure 4 – figure supplement 2. Gabapentin administration, but not chemogenetic activation of NPY-INs, induces conditioned place preference following spared nerve injury. (**A**) The experimental approach taken to generate the data presented in **B**. (**B**) Neither wildtype control nor AAV.flex.hM3Dq-mCherry spinal-injected NPY::Cre mice displayed a conditioned place preference (CPP) to i.p. CNO following SNI (n = 7; RM 2-way ANOVA). Data per individual mouse, also presented in Figure 4H. (**C**) The experimental approach taken to generate the data presented in **D**. (**D**) Wildtype mice display CPP to i.p. gabapentin administration following SNI (n = 6; *p = 0.016; paired t-test). Acc. = acclimation; Pre. = pre-conditioning; Con. = conditioning. Data are shown as individual matched values in (**B**) and individual values with mean ± SEM in (**D**).

Click here to enter text.

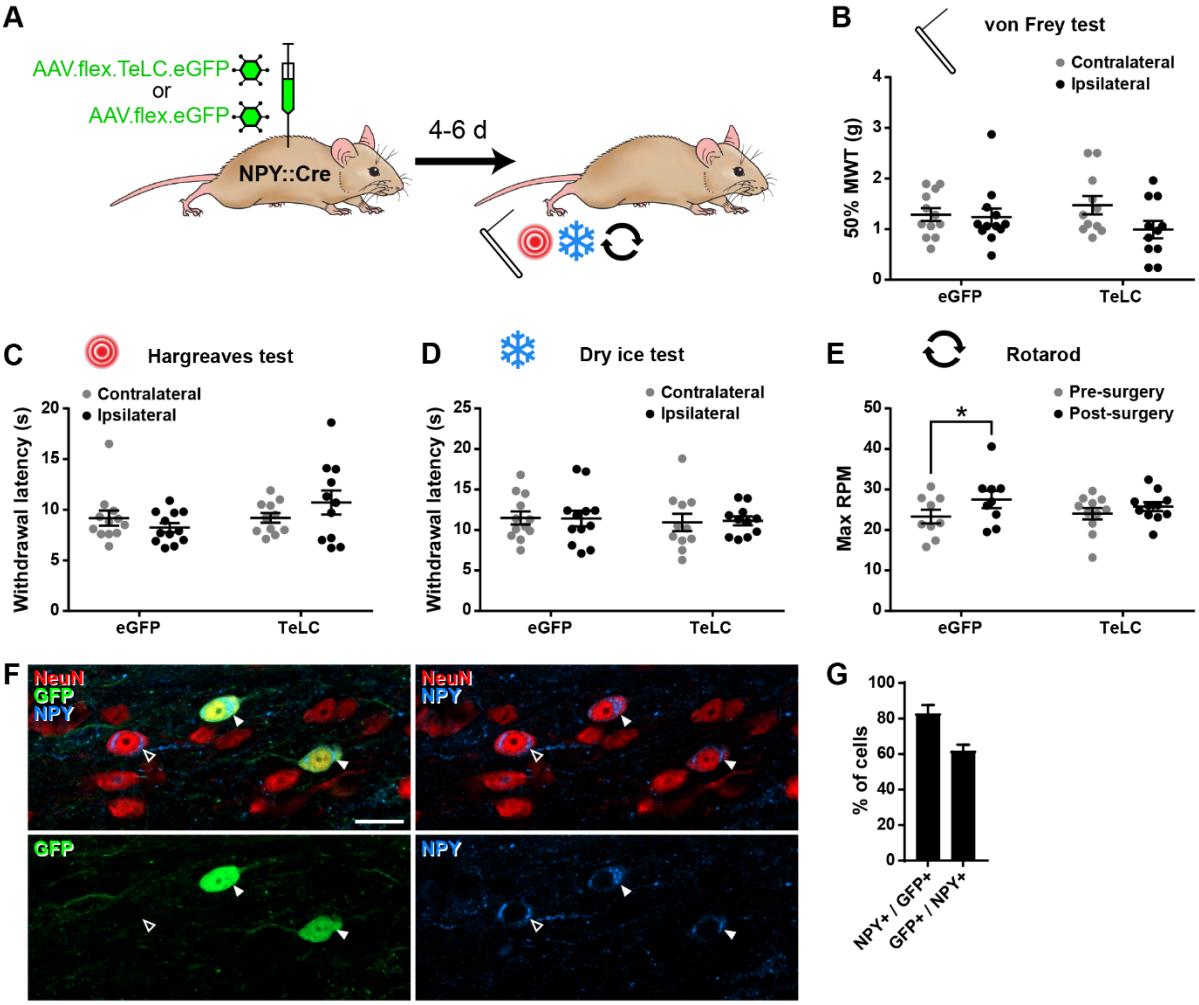

Figure 5 – figure supplement 1. Silencing of NPY-INs does not affect nociceptive thresholds. (**A**) The experimental approach used to generate data presented in this figure. (**B-D**) Results of mechanical (**B**), radiant heat (**C**) and cold (**D**) nociceptive testing of hindpaws of NPY::Cre mice ipsilateral and contralateral to spinal injections of AAV.flex.TeLC.eGFP or AAV.flex.eGFP carried out 4-6 days earlier. These analyses were performed on the same NPY::Cre mice as in Figure 5B-E (n = 12 for AAV.flex.eGFP, 11 for AAV.flex.TeLC.eGFP). No statistically significant differences were seen in any of the sensory modalities (repeated-measures 2-way ANOVA with Šidák's post-test). (**E**) Expression of TeLC and/or eGFP in NPY-INs did not impair motor co-ordination, as assessed by the accelerating rotarod test in the same NPY::Cre mice as above. A mild improvement in performance was observed in the AAV.flex.eGFP group compared to pre-surgery values, most likely reflecting a training effect (*p = 0.0137, repeated-measures 2-way ANOVA with Šidák's post-test). **(F)** Example confocal image (single optical section) from laminae II/II in the L4 segment of an NPY::Cre mouse that received spinal

1700 injections of AAV.flex.TeLC.eGFP. Two NeuN-immunoreactive cells (red) that co-
1701 express GFP (green) and NPY (blue) are marked with filled arrowheads. Another
1702 NPY-positive cell that does not express GFP is marked with an open arrowhead.
1703 Scale bar = 20 μm. **(G)** Quantification of the overlap between GFP and NPY
1704 immunoreactivity in laminae I-III of the L4 segment of 4 NPY::Cre mice that received
1705 spinal injections of AAV.flex.TeLC.eGFP. Data are shown as individual values with
1706 mean ± SEM in (**B-E**) and mean ± SEM in (**G**).

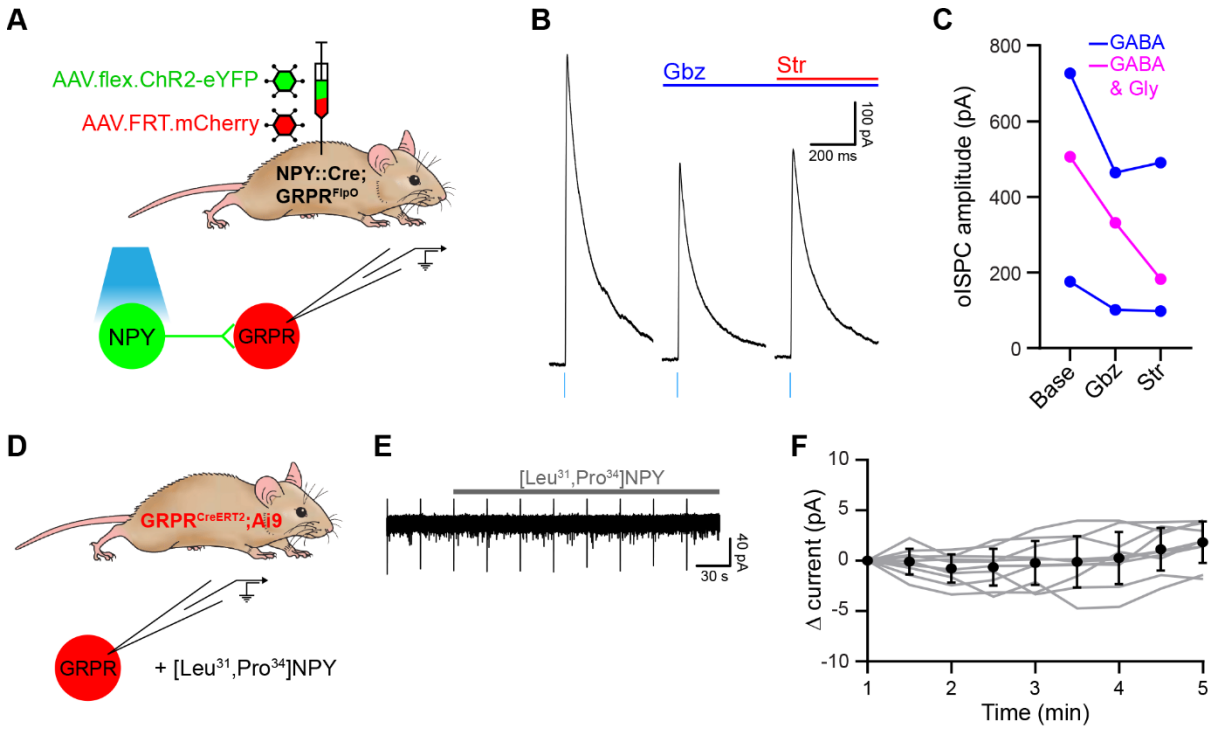

Figure 5 – figure supplement 2. NPY-INs generate GABAergic and glycinergic inhibition of GRPR-INs. (**A**) The experimental approach used to generate data presented in **B** and **C**. (**B**) Representative oIPSCs recorded in a GRPR-IN in the absence and presence of gabazine (Gbz) and strychnine (Str). Traces show an average of 6 stimuli, light blue bars denote period of optogenetic stimulation. (**C**) Quantification of the mean peak amplitude of oIPSCs recorded in the absence (Base) and presence of gabazine and strychnine. (**D**) The experimental approach used to generate data shown in **E** and **F**. (**E**) Representative trace recorded in a GRPR-IN prior to and during application of the NPY Y1R receptor agonist, [Leu^{31},Pro^{34}]-neuropeptide Y. (**F**) Quantification of the change in current recorded during the application of [Leu^{31},Pro^{34}]-Neuropeptide Y, compared to the mean current measured during the 1 minute baseline period. All cells tested (n=10) were classified as non-responders as they did not display an outward current of at least 5pA. Grey lines denote trajectories for individual cells, black dots and bars denote mean ± SD.

Click here to enter text.

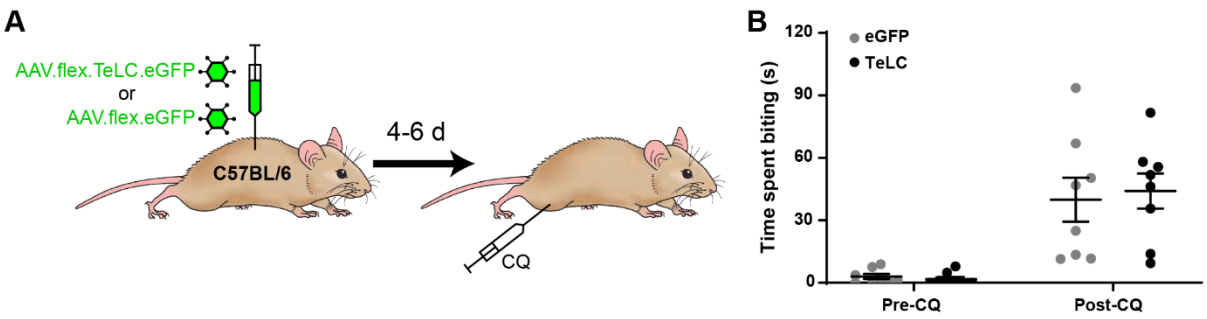

Figure 6 – figure supplement 1. Injection of AAV.flex.TeLC.eGFP does not cause exaggerated itch in wild-type mice. (**A**) The experimental approach used to generate data shown in **B**. AAV.flex.eGFP (eGFP) or AAV.flex.TeLC.eGFP (TeLC) were injected into the L3 segments of wild-type mice (n = 8 for both groups), and itch-related behaviour was assessed 4-6 days later. (**B**) No differences were observed in the time spent biting the calf between the eGFP and TeLC groups in the 30 minutes prior to (Pre-CQ) or following (Post-CQ) injection of chloroquine (p = 0.9891 and 0.8919, respectively, repeated-measures 2-way ANOVA with Šidák's post-test). Data are shown as individual values with mean ± SEM.